Population Balance Modeling of Agglomeration in Granulation Processes

by

Ola Maurstad

A dissertation submitted for the degree of doktor ingeniør

Department of Thermal Energy and Hydropower
Norwegian University of Science and Technology
Submitted February 2002

Summary

Agglomeration (the sticking together of particles) is often the major growth mechanism in granulation processes. The population balance equation (PBE) is a mathematical framework that is often applied to systems to describe how the particle size distribution changes as a function of time. Different kinetic terms are included in the PBE to describe the different particle growth mechanisms. In this work, a new kinetic model framework is proposed for the growth mechanism binary agglomeration. Binary agglomeration means that only two particles are involved in an agglomeration event. The generality of the new model framework is an advantage over the previous coalescence kernel framework. It is shown that an existing coalescence kernel model can be expressed by means of the new framework.

The new model framework is then adapted to the special case of fluidized bed granulation (FBG) by proposing/choosing expressions for the three submodels in the model framework. An advantage of the new FBG model is that a maximum number of agglomeration events per unit time can be estimated. This means that the model is one step closer to being used predictively. At the moment, no population balance models can predict granulation processes where agglomeration is the dominant growth mechanism. It is shown that both the new FBG model and an existing model could fit experimental data well, however, the new model reflects the situation that the presence of surface liquid is rate limiting for the agglomeration process.

Experiments in a laboratory batch fluidized bed granulator were carried out. Samples of the particle size distribution were taken at intervals during an experiment. These data were used to fit the model parameters of the FBG model. The dissertation includes a discussion of the effect of certain operating conditions such as bed temperature and liquid spray rate on a model parameter.

Acknowledgements

I wish to thank my academic supervisor Dr. Ing. Olav Bolland for his help and encouragement during the research. I am also thankful to Dr. Lian X. Liu and Dr. Jim Litster at the University of Queensland, Australia for all of their help during my six months in their group.

I acknowledge the assistance of Stewart Clark, English language advisor, Norwegian University of Science and Technology in the final round of editing this dissertation.

This work was supported financially by Norsk Hydro and the Research Council of Norway.

Contents

Summary i

Acknowledgements iii

Notation ix

1 Introduction 1
- 1.1 Fluidized Bed Granulation . . . 1
- 1.2 Scope of the Work . . . 2
- 1.3 Outline of the Thesis . . . 3

2 Review of the Literature 5
- 2.1 The Fluidized Bed Granulator . . . 5
- 2.2 Particle Movement . . . 5
  - 2.2.1 Fluidization . . . 5
  - 2.2.2 Movement of Single Particles . . . 7
- 2.3 Heat and Mass Transfer in Fluidized Beds . . . 8
- 2.4 Phenomena Changing the Particle Size . . . 10
  - 2.4.1 Layering . . . 11
  - 2.4.2 Agglomeration . . . 12
  - 2.4.3 Attrition and Breakage . . . 13
- 2.5 Binary Agglomeration . . . 14
  - 2.5.1 Interparticle Forces . . . 14
  - 2.5.2 Coalescence Theory . . . 15
- 2.6 Growth Regimes . . . 16
- 2.7 Experimental Studies of Fluidized Bed Granulation . . . 18
- 2.8 Numerical Simulations . . . 19
- 2.9 Population Balance Modeling . . . 20
  - 2.9.1 The Population Balance Equation . . . 21
  - 2.9.2 Binary Agglomeration . . . 22
  - 2.9.3 The Coalescence Kernel . . . 23
  - 2.9.4 Numerical Discretization Methods . . . 24

3 Kinetic Modeling of Binary Agglomeration 27
3.1 Introduction . . . 27
3.2 New Model Framework . . . 28
3.3 Modeling of $\dot{N}$ . . . 29
3.4 Modeling of $p_{j,k}$ . . . 35
3.5 Modeling of $\alpha_{j,k}$ . . . 36
3.5.1 A Qualitative Theory for $\alpha_{j,k}$ . . . 39
3.6 Summary of the Model Framework with Submodels . . . 41
3.6.1 Discretized Form . . . 41
3.6.2 Continuous Form . . . 41
3.7 Using the New Model Framework to Express a Coalescence Kernel Model . . . 42
3.8 Numerical Method . . . 43

4 Experimental Work 45
4.1 Introduction . . . 45
4.2 Experimental . . . 46
4.2.1 Experimental Apparatus . . . 46
4.2.2 Particulate Material and Granulating Liquid . . . 46
4.2.3 Procedure . . . 46
4.2.4 Sampling . . . 47
4.2.5 Drop Size Measurements . . . 48
4.3 Results and Discussion . . . 48
4.3.1 Effect of Spray Rate and Drop Size . . . 49
4.3.2 Effect of Bed Temperature . . . 49
4.3.3 Effect of Binder Concentration . . . 49
4.3.4 Stages in Fluid Bed Agglomeration . . . 51
4.3.5 Different Initial Bed Charges . . . 51
4.3.6 Breakage and Attrition . . . 55
4.4 Conclusions . . . 57

5 Simulation and Fitting of Model Parameters 59
5.1 Introduction . . . 59
5.2 Challenges in Comparing Simulation Results with Experimental Data . . . 60
5.3 The New and the Old Model . . . 61
5.4 Estimates of $\dot{N}_{\max}$ and $m_{\text{event,min}}$ . . . 66
5.5 The Effect of the Spray Rate . . . 69
5.6 The Effect of the Bed Temperature . . . 72
5.6.1 Estimates of a Particle's Drying Time . . . 75
5.7 Simulation of Experiment E2 . . . 78

6 Conclusions and Recommendations **83**
6.1 Conclusions 83
6.2 Recommendations for Further Work 84

List of References **87**

Notation

Latin Symbols

A	surface area [m^2]
a	half separation distance [m]; model parameter [-]
B_{aggl}	birth term, binary agglomeration [#/(m^3s)]
B_{nucl}	birth term, nucleation [#/(m^3s)]
b	model parameter [-]
C_p	specific heat capacity at constant pressure [J/(kgK)]
c	binder concentration [g PVP/ g water]
c_{l}	liquid heat capacity [J/(kgK)]
c_{p}	particle heat capacity [J/(kgK)]
$\mathcal{D}$	binary diffusion coefficient [m^2/s]
D_{aggl}	death term, binary agglomeration [#/(m^3s)]
D_{nucl}	death term, nucleation [#/(m^3s)]
d	diameter [m]
$\bar{d}$	average sieve diameter in a size fraction [m]
e	coefficient of restitution [-]
F_{dyn}	dynamic liquid bridge force [N]
F_{stat}	static liquid bridge force [N]
$f_{\text{a},j}$	area fraction of particles in size interval j [-]
$f_{\text{a},k}$	area fraction of particles in size interval k [-]
$f_{\text{a}}(u)du$	area fraction of particles in size range $(u, u+du)$ [-]
$f_{\text{a}}(v)dv$	area fraction of particles in size range $(v, v+dv)$ [-]
f_{drift}	ratio of drift volume to bubble volume [-]
f_{wake}	ratio of wake volume to bubble volume [-]
$G(v)$	layering growth rate [m^3/s]
H	bed height [m]
H_{mf}	bed height at minimum fluidization [m]
h	heat transfer coefficient [W/(m^2K)]; thickness of surface layer [m]
h_{a}	characteristic height of surface asperities [m]
k	heat conductivity [W/(mK)]
k_{g}	mass transfer coefficient [m/s]
Le	Lewis number
M	number of size intervals

M	effective average particle mass [kg]
$M_{j,k}$	effective average particle mass [kg]
M^*	critical effective average particle mass [kg]
m^*	largest mass of a particle capable of successful agglomeration with another particle of equal size [kg]
m	mass [kg]
$m_{\mathrm{drop}}(x)$	mass of a drop with volume x [kg]
m_{event}	liquid mass sprayed per potential agglomeration event [kg]
$m_{\mathrm{event,min}}$	theoretical minimum value of m_{event} [kg]
m_{l}	mass of liquid [kg]
m_{p}	mass of particle[kg]
m_j	representative particle mass of size interval j [kg]
m_k	representative particle mass of size interval k [kg]
$\dot{m}_{\mathrm{H_2O}}$	evaporation rate of water [kg/s]
$\dot{m}_{\mathrm{spray}}$	liquid spray rate [kg/s]
N	number of particles [#]
$\dot{N}$	number of potential agglomeration events per unit time [#/s]
$\dot{N}_{\mathrm{max}}$	maximimum number of agglomeration events per unit time [#/s]
$\dot{N}_{\mathrm{succ}}$	number of successful agglomeration events per unit time [#/s]
N_i	particle number in size interval i [#]
N_j	particle number in size interval j [#]
N_k	particle number in size interval k [#]
N_{t}	total particle number in granulator [#]
Nu	Nusselt number
$n(v)$	particle number density [#/m^3]
$\dot{n}_{\mathrm{in}}(v)$	flow rate of particles into system [#/(m^{3}s)]
$\dot{n}_{\mathrm{out}}(v)$	flow rate of particles out of system [#/(m^{3}s)]
Pr	Prandtl number
$p_{j,k}$	probability of a potential agglomeration event involving particles from size intervals j and k [-]
$p(u,v)dudv$	probability of a potential agglomeration event involving particles from size ranges $(u, u+du)$ and $(v, v+dv)$ [-]
$\dot{Q}_{\mathrm{conv}}$	heat transfer rate by convection [J/s]
q	integer value ≥ 1
$q_3(x)$	mass density distribution [-]
R	radius of sphere [m]
Re	Reynolds number
r_1	liquid bridge meridional radius of curvature [m]
r_2	liquid bridge neck radius [m]
S	ratio of liquid mass sprayed and initial bed mass/charge [-]
Sc	Schmidt number
Sh	Sherwood number
$\mathrm{St_v}$	viscous Stokes number

$\mathrm{St}_{\mathrm{v}}^{*}$	critical viscous Stokes number
T_{air}	air temperature [°C]
T_{bed}	bed temperature [°C]
T_{l}	liquid temperature [°C]
T_{p}	particle temperature [°C]
t	time [s]; bed turnover time [s]
U	superficial gas velocity/ fluidization velocity [m/s]
U_{mf}	minimum fluidization velocity [m/s]
u	particle volume [m^3]
V	ratio of initial liquid volume binding the particles and some mean particle size (see Section 3.5.1) [-]
v	velocity [m/s]; particle volume [m^3]
v_i	lower particle volume of size interval i [m^3]
v_{i+1}	upper particle volume of size interval i [m^3]
W	effective average particle volume [m^3]
W^*	critical effective average particle volume [m^3]
w^*	largest volume of a particle capable of successful agglomeration with another particle of equal size [m^3]
x	particle volume [m^3]
x_i	representative particle volume of size interval i [m^3]
x_j	representative particle volume of size interval j [m^3]
x_k	representative particle volume of size interval k [m^3]
Y	fraction of gas flow in excess of minimum fluidization appearing as bubbles

Greek Symbols

$\alpha_{j,k}$	probability of successful agglomeration [-]
$\alpha(u,v)$	probability density of successful agglomeration [-]
β_0	size-independent coalescence kernel [s^{-1}]; rate constant [s^{-1}]
$\beta(u,v)$	coalescence kernel, continuous form [s^{-1}]
$\beta_{j,k}$	coalescence kernel, discretized form [s^{-1}]
Δh	heat of evaporation [J/kg]
ΔP	pressure difference between gas and liquid [Pa]
$\delta_{j,k}$	Kronecker delta (1 if $j=k$, 0 if $j\neq k$)
ϵ_{app}	apparent fractional voidage [-]
η	fraction (defined by Equation (2.24))
γ	surface tension [N/m]
μ	dynamic viscosity [kg/(ms)]
ρ	density [$\mathrm{kg/m}^3$]
$\rho_{\mathrm{H_2O}}$	density of water vapor [$\mathrm{kg/m}^3$]
$\rho_{\mathrm{H_2O}}^{*}$	density of water vapor at liquid interface [$\mathrm{kg/m}^3$]

Abbrevations

DEM	discrete element method
FBG	fluidized bed granulation
LHS	left hand side
PEPT	positron emission particle tracking
PSD	particle size distribution
RHS	right hand side

Chapter 1

Introduction

1.1 Fluidized Bed Granulation

Fluidized bed granulation (FBG) is a process that belongs to the field of *particle technology*. "Particle technology is the study of discrete elements—bubbles, drops, and particles—the way in which they interact to produce a collective effect" [73]. FBG is a size enlargement process with applications including fertilizers, industrial chemicals, agricultural chemicals, pharmaceuticals, and a range of coating processes [81, pp. 20-77]. The goal of FBG is to produce solid particles with certain desired properties depending on the application. Two important growth mechanisms that are discussed in more detail in the next chapter are identified in the FBG process: *layering* and *agglomeration*. Layering is the gradual growth of particles due to solid deposition on their surfaces from the liquid spray, while agglomeration is the sticking together of two particles or more into a larger solid particle called an agglomerate.

Several terms exist in the literature that can all be covered by the above definition of FBG. Iveson et al. [29] refer to a FBG process where agglomeration is the major growth mechanism as a *wet granulation process*. Granulation is used synonymously with agglomeration. The reason probably is that agglomeration is the dominant growth mechanism in most other granulation processes. Uhlemann [85] uses the term *fluidized bed spray granulation* to describe FBG processes where layering is the desired growth mechanism. This seems to be common in German literature [21]. Nienow [50] does not include fluidized bed coating in the definition of FBG, as coating and layering processes are defined slightly different. It is argued that a coating process results in lower growth rates and more coherent coatings than a layering process. However, the surface morphology of the coating is not studied in the present work. Here, the most important aspect is to predict particle size. Therefore fluidized bed coating can also be included in the

general term FBG.

1.2 Scope of the Work

Several properties, such as size, shape, and porosity of the particles produced can be important. Size is probably often the most important one. Kinetic models predict how the particle size distribution (PSD) changes as a function of time. Such models would be very useful for controlling the growth process in a *fluidized bed granulator* if they could be used predictively. Good models could also help in scaling up. In addition, the industrial practitioner could gain understanding of what goes on inside the "black box" granulator.

The increase in particle size is due to the growth mechanisms of layering and agglomeration. Good models of the layering growth rate exist (see Section 2.9.1). However, the kinetic modeling of agglomeration (sticking together of solid particles) is more difficult. Agglomeration can occur as either nucleation (one agglomeration event involving three or more particles) or binary agglomeration (one agglomeration event involving two particles). In the case of nucleation, workers have found a close relationship between the drop size and the size of the particle formed (see Section 2.4.2). Therefore, the growth kinetics could, in principle, be determined from knowledge of the spray rate and the drop size distribution. This work is concerned with the kinetic modeling of binary agglomeration in the FBG process. That is, modeling the evolving particle size distribution as a function of time.

Today, no a priori models are available for the prediction of the evolving particle size distribution due to binary agglomeration in a FBG process, or any other wet granulation process. The existing models all use a number of model parameters (often three) that are unknown and must be fitted to experimental data. This means that the models cannot be used predictively. A good general model framework should have a structure so that the important parts of the overall problem (to predict particle size) are identified. These parts may be called submodels. The model framework consists of its submodels. Each of the submodels must then be expressed. Ideally, all of them should be known functions of material properties (e.g. viscosity and surface tension of the liquid, particle size, and wetting characteristics) and variables describing the operating conditions (e.g. liquid spray rate, bed temperature, and gas velocity). Unfortunately, these relations are unknown today. That is why the submodels contain model parameters with unknown values. These parameters should at least be qualitatively related to physics, because then the challenge of developing predictive submodels would be identified. Such predictive expressions could for example be functions of

dimensionless groups which incorporate material properties and operating conditions. A good model framework will point out the important problems and highlight the need for physical modeling of specified problems. This work proposes a new model framework for binary agglomeration. It is also adapted to the special case of FBG.

1.3 Outline of the Thesis

In Chapter 2, a literature review is given on topics related to FBG. The process is introduced and its physics discussed. A selection of experimental studies of FBG and the theory of population balance modeling are reviewed.

A new population balance model framework for binary agglomeration is proposed in Chapter 3. The new model framework is general in its form and has potential use in the description of any binary agglomeration process. The three submodels are then chosen so that the model becomes specific for the analysis of FBG.

Chapter 4 summarizes the experimental work carried out. FBG experiments were done in a batch fluidized bed granulator. The effect of the operating conditions are discussed. Different stages or regimes of the granulation process are identified.

In Chapter 5 the new model for FBG is discussed with a comparison of simulation results and experimental data. The model parameters are fitted to the experimental data, and a qualitative analysis of their dependence on liquid spray rate and bed temperature is given. Two of the model parameters are shown to determine the final, critical PSD in a case where the agglomeration process stops in a long experiment.

The conclusions and recommendations for future work are summarized in Chapter 6.

Chapter 2

Review of the Literature

The goal of this chapter is to review previous work dealing with the physics of a fluidized bed granulator. Existing experimental and modeling work on the kinetics of the fluidized bed granulation process is also reviewed.

2.1 The Fluidized Bed Granulator

The solid particles are processed inside a container, usually of cylindrical form (see Figure 2.1). At the bottom is an air distribution plate. An upward-flowing hot air stream comes through this plate which fluidizes (see the next section) the bed of particles. If the air velocity is too high, the particles can be blown out of the container. Filters and cyclones are often used to capture small particles from the outlet air flow. A liquid binder is normally sprayed on to the bed of particles from above (top-spraying) with a nozzle. This liquid could be a solution, melt or slurry. In case of a solution, the hot air will lead to the evaporation of the solvent. The presence of liquid is essential for the particles to increase in size. If the process is run as a continuous operation, there are inlets and outlets for particles. In case of a batch process, there are none.

2.2 Particle Movement

2.2.1 Fluidization

Kunii and Levenspiel define fluidization as the operation by which solid particles are transformed into a fluid-like state through suspension in a gas or liquid [37, p. 1]. When the fluid is passed upward through a bed of particles at a low flow rate, the particles are not moving. It is a fixed bed. At the minimum fluidization velocity, U_{mf} a point is reached where the particles are just suspended. This means that the frictional force from the fluid just counterbalances the weight of the particles. Smooth or par-

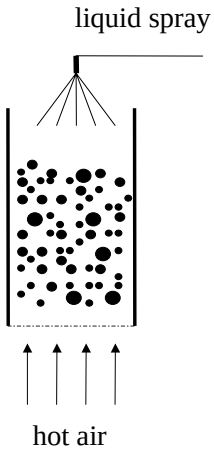

Figure 2.1: The fluidized bed granulation process

ticulate fluidization refers to the flow regime where a further increase in fluidization velocity (above minimum fluidization) results in a bed where the distribution of particles is spatially uniform [11, p. 4]. This has been observed for liquid-solid systems. Gas-solid systems (more relevant to granulation) will, generally, behave quite differently. Aggregative regimes such as bubbling or slugging fluidization are observed with increasing gas velocity. The presence of gas voids with almost no solid content are common for these regimes. Such a void is called a bubble. Bubbles form near the distribution plate and rise up through the bed, coalescing and increasing in size. When the size of a bubble is so large that it spreads across the vessel, it is called a slug. Bubbling and slugging regimes have been subjected to much research effort [10, p. 73]. Fluid bed granulators are operated in the bubbling bed regime.

The fluidization phenomenon is very much dependent on the material properties of the solid particles. Geldart [17] proposed a powder classification diagram for fluidization by air. The behavior of powders fluidized by gases falls into four categories characterized by density difference (between particle and gas) and mean particle size. Group A particles exhibit dense phase expansion after minimum fluidization and prior to the onset of bubbling. Group B particles bubble at the minimum fluidization velocity. Group C particles are cohesive and difficult to fluidize. Group D particles are of large size and/or density.

2.2.2 Movement of Single Particles

In a fluidized bed the bubbles cause movement of the solid particles. A higher fluidization velocity results in more bubbles. This leads to a higher rate of particle mixing. The movement of a single particle in a bubbling fluidized bed is complex and irregular. However, on the whole, certain circulation patterns will exist (see Figure 2.2).

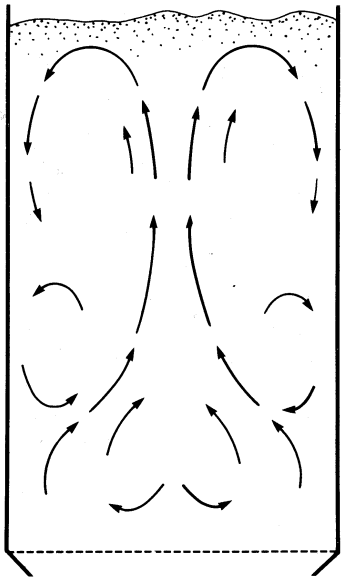

Figure 2.2: An example of a circulation pattern in a deep, bubbling fluidized bed [37, p. 140].

Baeyens and Geldart [4, p. 107] derived a theoretical expression for the bed turnover time:

$$t = \frac{H_{\mathrm{mf}}}{(f_{\mathrm{wake}} + 0.38 f_{\mathrm{drift}}) Y (U - U_{\mathrm{mf}})} \tag{2.1}$$

The physical basis of this equation is that particles move upwards in the wake and drift of bubbles (see Figure 2.3), and downwards elsewhere. A wake is defined as the the solids occupying the bottom of the bubble's completed sphere. The drift is the region behind the wake. Particles in the wake are assumed to move with the same velocity as the bubble, whereas particles in the drift only move with 38 % (empirically obtained) of this velocity. f_{wake} and f_{drift} are the ratios of the wake volume to the bubble volume and the drift volume to the bubble volume, respectively. The factor Y is a number less than unity, representing the fraction of the gas supplied in excess of minimum fluidization $[A(U - U_{\mathrm{mf}})]$ that appear as bubbles.

The parameters needed (f_{wake},f_{drift},Y) are supplied as a function of the Archimedes number.

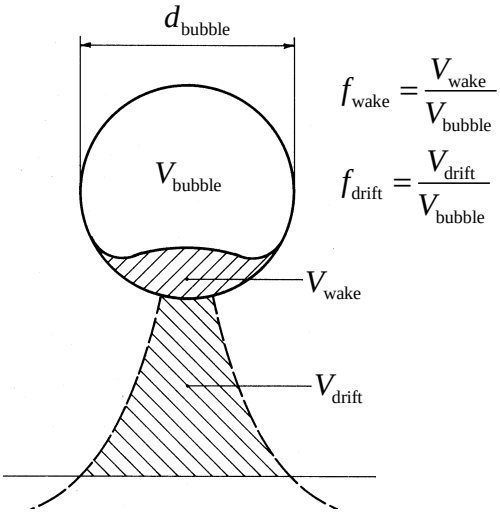

Figure 2.3: A bubble with its wake and drift. Adapted from [4, p. 99].

In a study by Stein et al. [82] a non-invasive technique called positron emission particle tracking (PEPT) was used to determine the solids flow pattern, solids circulation frequency, average upward velocity of particles, and characteristic times of particle motion. Two fluidized beds were studied. The first had an inner diameter of 70 mm and a bed height of 430 mm. The second had a diameter of 141 mm and a bed height of 600 mm. The material used was resin beads with an average size of 0.66 mm and a density of 1100 kg/m^3. These particles belong to Group B in Geldart's classification [17]. For the large bed, it was found that particles move upwards in the central part of the bed, downwards near the wall, and both upwards and downwards in the distributor region. The up-and-down movement is explained by particles moving upwards in the wake and drift of bubbles, and downwards elsewhere. Lateral mixing occurred mainly at the top of the bed where bubbles burst and near the distribution plate where bubbles form.

2.3 Heat and Mass Transfer in Fluidized Beds

In a fluidized bed, a large area of solid surface per unit particle mass is exposed to the gas. The smaller the particles are, the larger is the specific surface area of the particles. This large specific surface area facilitates

solid-to-gas heat and mass transfer, and is an advantage of the fluidized bed compared with other modes of contacting (e.g. a fixed bed or a rotary cylinder)[37, p. 10].

Ranz and Marshall [63, 64] proposed the following empirical correlations for heat and mass transfer for flow around a liquid drop:

$$\mathrm{Nu} = 2.0 + 0.60\ \mathrm{Re}^{\frac{1}{2}}\mathrm{Pr}^{\frac{1}{3}} \tag{2.2}$$

$$\mathrm{Sh} = 2.0 + 0.60\ \mathrm{Re}^{\frac{1}{2}}\mathrm{Sc}^{\frac{1}{3}} \tag{2.3}$$

The above equations are examples of the analogy between heat and mass transfer, which is valid for low mass transfer rates. The analogy exists owing to the fact that conduction and diffusion in a fluid are governed by physical laws of the same mathematical form [48, p. 844]. If a correlation for the Nusselt number is known, the Sherwood number is obtained by replacing the Prandtl number by the Schmidt number. Using the stagnant film model, Paterson [61] showed in a simple way that the lower theoretical value of the Sherwood number is 2. A similar analysis gives the same result for the Nusselt number.

As a first approximation the Lewis number (Le=Pr/Sc) equals unity for the system air and water vapor. The above equations then give Nu=Sh, which is equivalent to:

$$\frac{hd}{k} = \frac{k_g d}{\mathcal{D}} \tag{2.4}$$

Using the assumption that Pr=Sc and Equation (2.4), the ratio of the heat transfer coefficient and the mass transfer coefficient is obtained:

$$\frac{h}{k_\mathrm{g}} = \rho C_p \tag{2.5}$$

All physical properties of the fluid should be evaluated at the so-called film temperature, which is defined as the average temperature of the surface and the bulk of the approaching stream of fluid.

As pointed out by Martin [46], there are no generally accepted principles for calculating heat and mass transfer in fluidized beds. Difficulties with experimental techniques and interpretation of results lead to much scatter in published data [37, p. 258]. An interesting point is that both the Nusselt and Sherwood numbers, as measured experimentally, are lower than the theoretical minimum 2 for a single sphere at low Reynolds numbers. Brodkey et al. [9] argue that Nu cannot be lower than 2, even in the case of a fluidized bed. The reason is that the presence of neighboring particles facilitates transfer due to effects such as removal of the boundary layer under collisions and generation of turbulence by the motion of bubbles.

Using an experimental technique together with a model for fluidized bed heat transfer, Nusselt numbers 20-100 times higher than those for a single sphere were obtained.

Jonassen [30] investigated the heat transfer to an immersed heat exchanger in a fluidized bed dryer. By using differential pressure probes with a new signal processing technique, important bubble parameters were estimated. A new parameter termed the bubbling intensity was found to be important for the heat transfer coefficient.

Maronga and Wnukowski [45, 44] investigated the air temperature and humidity profiles in a fluidized bed coating process with top-spraying. Four different zones were identified: a spraying zone, a drying zone, a non-active zone, and a heat transfer zone. The spraying zone is the upper part of the bed where the particles are hit by the liquid drops and the air has maximum humidity. Below this zone, is the drying zone. Here, large fluctuations in temperature and humidity are observed (indicating drying). Then, further down in the bed follows the non-active zone where the temperature and humidity have constant values. At the bottom, next to the distribution plate, is the heat transfer zone. Here, the gas temperature is higher than that in the non-active zone. The sizes of the different zones are functions of material properties and operating conditions.

Heinrich and Mörl [21, 20] used mass and energy conservation equations to describe the mass and heat transfer in an FBG process. The discretized counterparts of these differential equations describe mass and energy balances on a small volume element in the granulator. By solving the system of equations, plots of air moisture, air temperature, degree of wetness of the particles (fraction of wet surface), liquid film temperature, and particle temperature can be depicted as functions of the radial and axial positions in the cylindrical bed. Radial and axial dispersion coefficients are used in the conservation equations. These coefficients cannot be determined a priori, but must be fitted to experimental data to predict the observed behavior.

2.4 Phenomena Changing the Particle Size

The different phenomena responsible for changes in particle size will now be discussed. In the literature, the terms used to describe these phenomena are often used differently by various authors. Therefore, for each phenomenon, the term used in this dissertation is first defined based on my understanding, and then the reviewed literature is discussed. The term *growth rate* is used to describe the overall rate of increase in particle size and is here defined as the increase in the mass mean diameter per unit time.

2.4.1 Layering

In this work, layering is defined as the gradual increase in particle size due to the build-up of solid on a particle surface, which results from the transition of liquid spray drops to solid material.

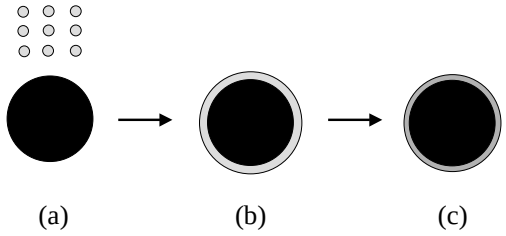

Figure 2.4: The layering growth mechanism. (a) One or more drops hit and adhere to a solid particle. (b) The liquid wets the particle totally or partially. (c) The solvent evaporates and leaves solid material on the surface.

Nienow uses both the term layering and coating [50]. In his definition, layering includes the formation of bonds to other particles which subsequently break, whereas coating does not include this situation. The consequence of this definition is that coating represents a smoother and more even solid deposition on particle surfaces than layering. Link and Schlünder [40, 39] investigated the layering mechanism on a single freely suspended particle. It was pointed out that the adhesion probability of liquid drops on the solid particle determines the growth rate. Many variables of importance for the adhesion probability were studied. Wnukowski [90] modeled growth by layering in a fluidized bed coating process where layering/coating is the wanted growth mechanism. A two-zone model was proposed to describe the growth process. Layering takes place in the upper zone, while no growth happens in the lower zone. Both zones are modeled as perfectly mixed, with certain exchange rates between the zones. It was shown that this model could explain the distribution of coating thicknesses found in experiments. It is, however, difficult to validate the rates of exchange between the two zones. Perhaps the PEPT could be used. Maronga [44] later extended this model to include one more zone. Heinrich [20, p. 42] used population balances to model a continuous type FBG process where layering was the important growth mechanism. The model took both particle size and the particle density into account because the layered material in general has another density than that of the original particle.

2.4.2 Agglomeration

Agglomeration is the case when solid particles stick together because of attractive forces, and form a larger particle. Agglomeration can happen as binary agglomeration or nucleation. To understand the kinetics of agglomeration it is important to distinguish between the two. This is often not the case in the literature.

Nucleation:
When three or more solid particles are involved in an agglomeration event, the term nucleation is used.

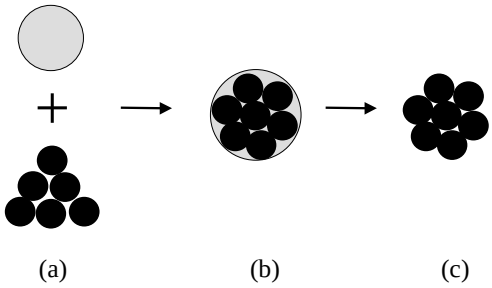

Figure 2.5: The binary agglomeration mechanism. (a) A large drop hit several particles. (b) A large agglomerate is formed. (c) The solvent evaporates.

Waldie [87] studied the nucleation mechanism where one single liquid drop engulfs several solid particles. A close relationship between drop size and the resulting agglomerate was found. Larger drops resulted in larger agglomerates. Schaafsma et al. [66] developed a new nozzle capable of producing mono-sized drops. This was used in fluidized bed granulation experiments, and a linear relation between the number of drops of which an agglomerate consists and its volume was found. A nucleation ratio factor introduced can be understood as the ratio of the volume of the agglomerate and the liquid necessary to form it. This factor is a function of the material properties of the liquid and the solid particles.

Binary Agglomeration:
When only two solid particles are involved in an agglomeration event, the term binary agglomeration is used. Binary agglomeration is discussed in more detail in Section 2.5

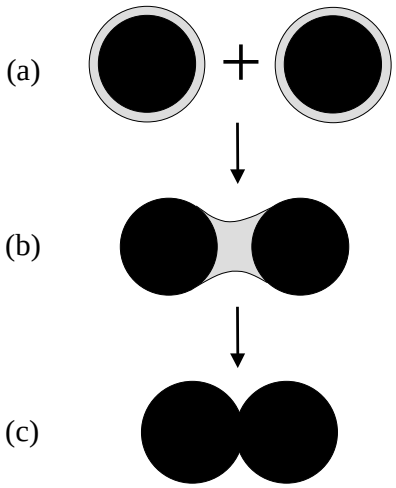

Figure 2.6: The binary agglomeration mechanism. (a) At least one of the two particles are surface wet. (b) A liquid bridge arises upon contact. (c) If the attractive force is strong enough to prevent separation, a solid bridge is formed.

2.4.3 Attrition and Breakage

Attrition is defined here as the gradual break-down of the solid particle surface, which leads to the generation of fine dust. *Breakage* is defined here as the sudden fracture of a solid particle/agglomerate into a few large fragments.

Stein et al. [83] studied the attrition of porous glass particles in a fluidized bed. For a multi-orifice distributor, the attrition rate was found to be roughly proportional to the excess gas velocity. Werther and Reppenhagen [89] investigated "attrition" (defined as both attrition and breakage) in a fluidized bed, and proposed a priori models for different mechanisms such as grid jet attrition, bubble-induced attrition, and attrition in the cyclone. Mishra and Thornton [49] used numerical simulations based on the discrete element method (DEM) to examine the breakage of agglomerates. Shamlou et al. [75] studied "breakage"(defined as both attrition and breakage) in a fluidized bed experimentally, and proposed models for the attrition of particles due to particle-particle and particle-wall impacts.

2.5 Binary Agglomeration

2.5.1 Interparticle Forces

The attractive interparticle force of practical importance in most granulation processes is that of liquid bridges (see Figure 2.7). Seville [74] shows that other interparticle forces like van der Waals forces and electrostatic forces may be one or more orders of magnitude less than the static force of a liquid bridge. Liquid bridges may be formed if surface liquid is present near the point of contact between two particles. The liquid in a bridge may be converted (e.g. by evaporation of the solvent) to a solid bridge. Liquid bridges exhibit both dynamic and static forces and are energy dissipative [74]. The static liquid bridge force (or capillary force) is a sum of the surface tension force and the force arising from the suction pressure in the liquid bridge [74, 76]:

$$F_{\text{stat}} = 2\pi r_2 \gamma + \pi r_2^2 \Delta P \tag{2.6}$$

where ΔP is given by the Young-Laplace equation:

$$\Delta P = \gamma \left(\frac{1}{r_1} - \frac{1}{r_2} \right) \tag{2.7}$$

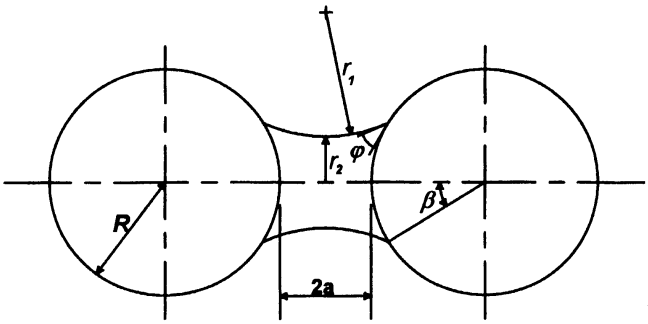

Figure 2.7: Liquid bridge between to spheres of equal size [74].

The dynamic force (or viscous force) in the liquid bridge will always oppose relative movement of the two particles. The two particles could be moving towards each other (see Figure 2.8), or they could be on the rebound after a collision. An approximate expression for this force is [74]:

$$F_{\text{dyn}} = \frac{6\pi\mu R^2 v}{a} \tag{2.8}$$

More work on liquid bridges is done by Ennis et al. [16] and by Simons and Fairbrother [77].

There are no conclusions in the literature to determine whether the static or the dynamic contribution is most significant in fluidized bed granulation. This is reflected in the different coalescence models discussed in the next section, some focus on the viscous force, while others focus on the capillary force.

2.5.2 Coalescence Theory

The term *coalescence* is used here to describe the first stage of a binary agglomeration event. Two colliding particles coalesce if the liquid bridge formed is strong enough to prevent rebound after the collision. Even if coalescence is successful, the particle pair may be broken apart by subsequent impacts from other particles so that the agglomeration event is unsuccessful. However, coalescence must be successful for the agglomeration event to be successful.

Ennis et al. [14] analyzed the impact of two solid, non-deformable spheres, each of which is covered by a thin liquid layer (see Figure 2.8). If the collisional kinetic energy is dissipated by the viscous liquid and elastic losses in the solid, successful coalescence will take place. Mathematically, the collision is successful (coalescence does happen) if the viscous Stokes number,

$$\mathrm{St_v} = \frac{8\rho v R}{9\mu} \tag{2.9}$$

is less than the critical viscous Stokes number:

$$\mathrm{St_v^*} = \left(1 + \frac{1}{e}\right) \ln\left(\frac{h}{h_\mathrm{a}}\right) \tag{2.10}$$

It can be seen that a lower value of the coefficient of restitution, e and a higher value of the liquid layer thickness, h (both effects leading to more dissipation of the collisional kinetic energy) cause a higher value of the critical viscous Stokes number, $\mathrm{St_v^*}$. This means that the two colliding spheres may be larger or that their velocities may be higher, and still successfully coalesce.

Simons et al. [78] considered that coalescence would be successful if the particle collisional kinetic energy was below that required to break the liquid bridge arising on contact. A simple expression for the liquid bridge rupture energy was derived by them. While Ennis et al. ignore the capillary force, Simons et al. ignore the viscous force.

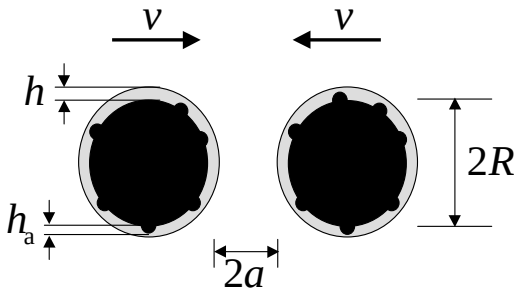

Figure 2.8: Schematic of two colliding spheres each of which is covered by a liquid layer of thickness h. The characteristic length scale of the surface asperities is h_a.

He [19] proposed another criterion for particle coalescence by collision. This criterion directly compares the forces involved in the course of a collision, instead of using energy conservation. However, no quantative validation of the concept was carried out.

Liu et al. [43] extended the Stokes analysis of Ennis et al. to include plastic deformation during collision. The model gives the condition for two types of coalescence. Type I coalescence occurs when the colliding particles coalesce by viscous dissipation in the surface liquid before their surfaces touch. Type II coalescence occurs when the two particles are slowed to a halt during rebound, after their surfaces have made contact. According to [81, p. 2064] a fluidized bed process is classified as a low agitation intensity process, and therefore deformation can be ignored to a first approximation. This means that the original model of Ennis et al. may describe a fluidized bed system as well as the extended model.

Lian et al. [38] simulated the collision between two agglomerates using the discrete element method (see Section 2.8). In these numerical experiments it was found that the energy dissipated was associated primarily with the viscous resistance of the fluid and the interparticle friction rather than by liquid bridge bond rupture.

2.6 Growth Regimes

Iveson et al. [29] point out that plots of the mass mean diameter versus time in wet granulation processes can show a number of characteristic regions. More work on factors determining growth behavior in wet granulation systems can be found in [28, 26, 27]. However, because the FBG process has

some special features like continuous spraying of liquid and simultaneous drying, the analysis of other wet granulation processes is not directly applicable. The most common growth regimes in an FBG process will therefore be defined here. One or more of the following regimes may occur in a given process:

- Nucleation regime
- Induction regime (no growth)
- Binary agglomeration regime
- Layering regime

The regimes are given the names of the dominating growth mechanism. The induction regime is a period of no growth, which is explained by surface dry particles. Smith and Nienow [79] observed this behavior for porous particles of alumina. The induction regime can also be identified in the growth curve shown in the work of Cryer [12]. It is therefore not correct that induction behavior has not been reported in fluidized beds, as claimed by Iveson et al. [29, p. 25].

A batch FBG process may enter all of the four mentioned regimes. Nucleation will dominate when the drop size is large compared to the particle size. Each drop results in a larger particle (agglomerate), and the growth rate is high. At some time the fine solid particles have all been used, so nucleation can no longer proceed. If the particles are porous and are not filled with liquid, drops may be sucked fast into the particles leaving their surface dry. Then induction behavior may be observed. Depending on spraying and drying conditions, it is possible that the porous particles may be later saturated with liquid, and the surfaces will again become wet. Growth may then continue with binary agglomeration. The growth rate in this regime is lower than in the nucleation regime. This is observed in the work of Schaefer and Worts [71, fig.2]. In the end, the attractive force of the liquid bridges may get too weak to keep the large particles together, and the layering regime is entered. This regime is characterized by a very low growth rate compared to agglomeration.

In actual industrial processes one combines the material properties of the liquid spray and the operating conditions (e.g. temperature, gas velocity, and drop size) in such a way that the required regime is dominant. One may for example wish to coat particles so that layering is the only mechanism, or one may want high growth rates and porous particles formed by agglomeration.

2.7 Experimental Studies of Fluidized Bed Granulation

This section reviews experimental studies of batch FBG. The most important growth mechanisms in these studies probably are a combination of nucleation and binary agglomeration. If the initial particles are small compared to the drop size, it is likely that nucleation will occur in the first stage of growth. As the particles increase in size and the drop size remains the same, binary agglomeration may take over as the dominant mechanism. Finally, the particle size distribution may reach a point where further growth can only take place through the layering mechanism.

In the 1970s, Ormos and co-workers [51, 56, 57, 58, 52, 53, 54, 55, 60, 59] wrote a series of articles on FBG. Schaefer and Worts [67, 68, 69, 70, 71] also carried out similar experiments in the same period. The effect of several process parameters and material properties on the growth rate were studied. A large drop size, a high liquid flow rate, and a low inlet air temperature were found to result in the highest growth rates [71]. All these effects sustain the presence of liquid, which acts as a glue, and therefore results in a higher agglomeration rate. A higher binder concentration (kg solute/ kg solvent) was also found to increase the growth rate. The effect was explained partly by a resulting larger drop size and partly by stronger liquid bridges [70].

Smith and Nienow [79] found that an increased excess gas velocity ($U - U_{\mathrm{mf}}$) resulted in a lower growth rate. This was explained with an increased frequency and intensity of collisions, tending to break the bonds between particles. A higher fluidization velocity will also cause a higher particle circulation rate (due to more bubbles), which may result in particles picking up less liquid in the spray zone, and could reduce the volume of the liquid bridges. Also, the drying rate is increased, and this means less surface liquid available for the formation of liquid bridges. A larger size of the initial particles was also found to shift the growth mechanism from agglomeration towards layering, resulting in a lower growth rate.

Becher and Schlünder [6, 5] examined the particle growth mechanism in a fluidized bed with a nozzle spraying upwards into it. If the desired growth mechanism is layering, they recommend a shallow bed, so that the air flow from the nozzle will form an upward jet penetrating the particle layer. This will create a drying zone (consisting of the jet and the region above the fluidized bed) for the wetted particles where the void fraction is large. By controlling the inlet air temperature and the gas velocity, it is possible to make sure most wetted particles are surface dry when they return from the drying zone and back to the bed. In this way, unwanted (in this case)

agglomeration can be avoided.

Schaafsma et al. [65] pointed out that the ratio of the spray rate and the surface renewal rate (the supply rate particles to the surface) determine the liquid distribution on the particles in the spray zone. In their experiments, the fluidization velocity was kept constant, so that the excess gas velocity decreased as the particles grew in size. Therefore, mixing was gradually reduced (lower rate of surface renewal), and overwetting of the surface would occur. At this time the experiment was stopped. In agreement with the previous mentioned studies, a larger drop size and a lower inlet air temperature were found to increase the agglomerate growth rate. A novel pulse spraying technique was proposed. The duration of each spraying pulse and the time between the pulses could be varied to control the relative humidity of the interstitial gas in the emulsion phase. If the relative humidity gets too high, adsorption of water molecules on the particles can cause an increase in interparticle attractive forces, and hence reduce mixing or cause defluidization.

2.8 Numerical Simulations

Recent numerical simulation methods for discrete particle systems like a fluidized bed include the two-fluid model (TFM) and the discrete element method (DEM) [33]. In the TFM the solid particles are considered as a continuous phase together with the gas phase. Such models are generally referred to as continuum models or the Eulerian approach [34]. Conservation equations and interaction terms for the coupling between the phases fully describe the system. Such models have been applied to the analysis of fluidized bed systems [8, 33, 72]. However, the DEM where the motion of each individual particle can be determined, seems to be a more promising technique. This is because of its few postulations and adjustable parameters compared to the TFM [33]. It should also be mentioned that DEM models could be used to develop closure laws for particle-particle and particle-wall interactions in continuum models [34]. The continuum models would then be useful to study flow phenomena at the macroscopic level.

There are two types of DEMs, based on the hard and soft particle approaches [38, 73]. In the hard particle approach, no overlap of particle surfaces is permitted. Particles interact by instantaneous collisions. This approach cannot easily deal with a dense particulate system (like a bubbling fluidized bed) [73]. In the soft particle approach interparticle collisions are treated as a continuous process that takes place over a finite time. The forces between two particles are calculated as functions of the distance between them and are based on particle-particle interaction models. This

approach has the potential to relate individual particle properties to the macroscopic behavior of the particle system. Extensive research is now being carried out in this field [84].

This may prompt the question of why DEM modeling is not used to simulate the whole fluidized bed granulation process. Even though the technique has a great potential in the future, it is today not useful for simulating a real FBG process. According to Seville [73], the maximum number of particles that can be handled with the current technology is up to about 10^7. In a small experimental FBG experiment (as described in Chapter 4), there is at the very least 10^8 particles. Even if the number of particles could be handled, there would still remain several problems. A fluidized bed granulation process is very complex, and it involves a good deal of physics that represents a challenge for DEM modelers, e.g.:

- Geometry of particles
- Liquid drops adhering to particles and wetting their surface
- Formation and strengthening of liquid bridges
- Heat, mass, and momentum transfer between particles and the surrounding gas
- Physical realistic particle-particle interaction laws

Another point is that a typical experiment lasts for hours, while the timesteps used in the numerical solution of DEM models are very short (e.g. $\leq 10^{-3}$ seconds). Seville [73] argues that the value of DEM probably is in carrying out "numerical experiments", which reveal important aspects of the behavior, not simulating the whole process with all its complexities.

As the main interest of this work is the kinetics of binary agglomeration in the FBG process, it was decided to work within the framework of population balance modeling, which has the purpose of describing the evolution of the particle size distribution as a function of time. This modeling technique is discussed in the next section.

2.9 Population Balance Modeling

Randolph and Larson describe the population balance as a number continuity equation in particle phase space [62, p. 54]. They define particle phase space as the least number of independent coordinates attached to a particle distribution that allow a complete description of the properties of the distribution. This simply means that the population balance is a tool for keeping

track of the number of particles and their properties (e.g. size and porosity). However, most models of granulation processes use one-dimensional population balances [25]. This means that the only coordinate/property assumed to affect growth behavior is size (particle volume). This assumption is also made in this work.

2.9.1 The Population Balance Equation

The population balance equation (PBE) is a mathematical description of how the particle size distribution changes as a function of time. Kinetic terms for all phenomena causing a change in the particle size distribution can be added in the PBE. The general PBE for an open system with layering, binary agglomeration and nucleation can be written:

$$\begin{aligned} \frac{\partial n(v)}{\partial t} + \frac{\partial (G(v)n(v))}{\partial v} &= B_{\text{aggl}}(v) - D_{\text{aggl}}(v) \\ &\quad + B_{\text{nucl}}(v) - D_{\text{nucl}}(v) \\ &\quad + \dot{n}_{\text{in}}(v) - \dot{n}_{\text{out}}(v) \end{aligned} \tag{2.11}$$

In this equation attrition and breakage are not considered. The number density function, $n(v)$ gives the number of particles in size range i when it is integrated over that discrete region:

$$N_i = \int_{v_i}^{v_{i+1}} n(v)dv \tag{2.12}$$

The layering growth rate, $G(v) = dv/dt$ can be modeled by assuming that the solid is deposited on the particles in proportion to surface area [20, p. 46]. Layering is modeled mathematically as a continuous process (the second term on the LHS of Equation (2.11)), whereas nucleation and binary agglomeration are discontinuous events that need to be modeled in another way. There are birth and death terms present on the RHS of Equation (2.11). That is because both nucleation and binary agglomeration can happen into (birth) and out of (death) a certain size interval. For nucleation in fluidized bed granulation there are no population balance models available in the literature. However, using the results from Waldie and Schaafsma et al. [87, 66] who found a close relationship between the drop size and the resulting agglomerate, it seems possible to develop a model. In such a model one would need to include two situations: the direct formation of an agglomerate from a drop (engulfement of fine particles) and binary agglomeration of larger particles. However, this idea is not pursued further in this work.

2.9.2 Binary Agglomeration

For a batch system with binary agglomeration only, Equation (2.11) is reduced to [2]:

$$\frac{\partial n(v)}{\partial t} = B_{\text{aggl}}(v) - D_{\text{aggl}}(v) \tag{2.13}$$

where,

$$B_{\text{aggl}}(v) = \frac{1}{2N_t}\int_0^v \beta(v-u,u)n(u)n(v-u)du \tag{2.14}$$

$$D_{\text{aggl}}(v) = \frac{1}{N_t}\int_0^\infty \beta(v,u)n(u)n(v)du \tag{2.15}$$

where the leading factor of 1/2 in the expression for $B_{\text{aggl}}(v)$ has been introduced to avoid counting agglomeration events twice. An alternative would be to change the upper limit of integration from v to $v/2$ and remove the factor of 1/2. The two last equations were introduced by Kapur and Fuerstenau [32] in a slightly different form. In their paper, the equations were written in discretized form. Also, β (later referred to as the coalescence kernel), was introduced as a product of a collision frequency and a probability of successful coalescence/agglomeration. Furthermore, the coalescence kernel was not taken to be a function of the size of the two colliding particles ($\beta(u,v) = \beta_0$), therefore the term random coalescence was used. If all particles in a granulator experience the same number of successful collisions with other particles per unit time, $\beta_0 N_j$ would be the number of agglomeration events including size interval j. However, only a fraction of these events would include particles from size interval k. Kapur and Fuerstenau take this fraction to be N_k/N_t, the number fraction of size interval k. They then obtain the following expression for the rate of agglomeration between particles from size intervals j and k:

$$\frac{dN_i}{dt} = \beta_0 N_j \frac{N_k}{N_t} \tag{2.16}$$

This equation can be understood as the rate of change of particle number in size interval i due to agglomeration between particles from size intervals j and k. The continuous Equations (2.14) and (2.15) can be written from knowledge of Equation (2.16). β_0 is, however, replaced with the more general coalescence kernel $\beta(u,v)$. Because the last equation is so much easier to read, this is chosen as the essential equation when going into discussion of the kinetic modeling of binary agglomeration. With the more general kernel one obtains:

$$\frac{dN_i}{dt} = \beta_{j,k} N_j \frac{N_k}{N_t} \tag{2.17}$$

2.9.3 The Coalescence Kernel

Within the framework of Equation (2.17), the challenge is to find the best expression for the coalescence kernel, $\beta(u,v)$[1]. Several kernels have been proposed in the literature, and a review is given in [81, p. 2087]. All kernels have a number of parameters that need to be fitted to experimental data, therefore no a priori prediction of agglomeration kinetics is possible today. However, these model parameters could in principle be linked to physical quantities, and this would be easier with the "right" kernel. This point provides a motivation for developing population balance models, even though they cannot be used in a predictive way today.

The simplest expression for the kernel is the model by Kapur and Fuerstenau [32], which only consists of one parameter:

$$\beta(u,v) = \beta_0 \tag{2.18}$$

A major assumption of this kernel is that the growth process takes place by random coalescence. This means that the size of the particles is not taken into account. The kernel is size-independent. Another assumption usually made is that the value of the parameter(s) is not a function of time. This implies that all process conditions are taken to be the same throughout the process. The work of Adetayo et al. [3] is an exception. They used a sequential kernel for two different growth stages in time.

Later, more complex, empirical expressions arose. These described the growth process as being preferential or non-random. This means that the size of the colliding particles are taken into account. For example, one kernel with three parameters was expressed [24]:

$$\beta(u,v) = \beta_0 \frac{(u+v)^a}{(uv)^b} \tag{2.19}$$

This and other kernels were pure empirical functions with no theoretical derivation. These kinds of kernels cannot be expected to predict agglomeration kinetics outside of the range of conditions in which the model parameters were fitted.

Adetayo and Ennis proposed a kernel where all collisions are taken as successful if the effective average particle volume is less than a critical value [1, 2]:

$$\beta(u,v) = \begin{cases} \beta_0 & \text{if} \quad W \leq W^* \\ 0 & \text{if} \quad W > W^* \end{cases} \tag{2.20}$$

[1] $\beta_{j,k}$ is the notation used for the discretized equivalent of $\beta(u,v)$

The effective average particle volume is defined:

$$W = \frac{(uv)^b}{(u+v)^{2b-1}} \tag{2.21}$$

The model parameters are β_0, b, and W^*. Even if Equation (2.19) and Equation (2.21) have similar form, the model of Adetayo and Ennis identifies two key areas of the overall problem: the collision frequency that may potentially lead to successful agglomeration and a criterion to determine if a specific combination of particle sizes will be successful. The concept of a critical effective average particle volume has a physical basis. A given attractive force will more easily be able to keep two small particles together than two large ones. The theoretical work of Ennis et al. [14] mentioned in Section 2.5.2 also shows this.

Cryer [12] proposed a new coalescence kernel for modeling binary agglomeration in a fluidized bed. The Stokes analysis of Ennis et al. (see Section 2.5.2) is used as the starting point. On the basis of distributions of particle sizes and collision velocities, a distribution of Stokes numbers is calculated at every timestep. The coalescence kernel is postulated to be proportional to the fraction of Stokes numbers below the critical Stokes number. To be able to predict different regimes of slow and rapid growth, the critical Stokes number is modeled as an empirical function of time with two model parameters. A weakness with this kernel is that it is size-independent, so it will wrongly predict the successful agglomeration of two very large particles as long as the kernel is non-zero. This makes the model unphysical and less general. Another weakness with Cryer's model is that a lot of effort is put into making an estimate for the collision velocities and its distribution (including both the use of empirical correlations and experimental measurements).

Because it is simpler, closer related to physics and more general (not specific for FBG), the model of Adetayo and Ennis is chosen as the basis for comparison for the new population balance model which is proposed in a later chapter.

2.9.4 Numerical Discretization Methods

A population balance equation can in most cases not be solved analytically. Therefore, a numerical method is required. Several discretization methods [22, 23, 35, 42] are available for the solution of Equation (2.13). The discretization procedure results in a system of ordinary differential equations. There will be one particle number conservation equation for each size interval, which states the rate of change of particle number due to agglomeration

into and out of that size interval:

$$\frac{dN_i}{dt} = \sum \text{Births} - \sum \text{Deaths} \tag{2.22}$$

The discretization methods differ in the way they split the size (particle volume) axis into size intervals (see Figure 2.9), and also in the way the birth and death terms in the above equation are represented.

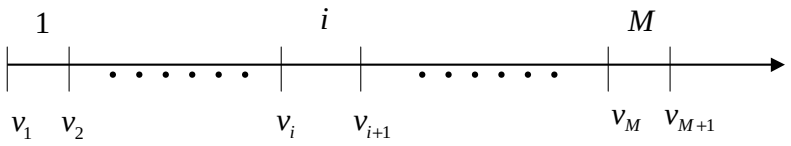

Figure 2.9: The size (volume) axis is divided into M size intervals. Each interval has a lower and an upper volume.

The method of Hounslow et al. [23] used a geometric grid ($v_{i+1} = 2v_i$) to determine the size intervals. This results in a very coarse grid, which can be a disadvantage. The expressions for the birth and death terms consist of four simple terms. Litster et al. [42] extended this method to allow the use of a finer geometric grid where $v_{i+1} = 2^{1/q} v_i$ and where the integer $q \geq 1$. The birth and death terms were now represented by six more complicated terms caused by the finer grid.

The method of Kumar and Ramkrishna [35] has the advantage that any type of grid can be chosen. In another version [36] it can also handle growth by layering very well because a moving grid is chosen. Here the previous methods that use stationary grids face considerable problems. The method of Kumar and Ramkrishna is also recommended by Vanni [86] in his review. This method is therefore chosen as the numerical method. The size axis is divided into small intervals. Size interval i contains the sizes between the lower limit v_i and the upper limit v_{i+1}. The particle population in a size interval (cell) is represented by a single size x_i (grid point) such that $v_i < x_i < v_{i+1}$.

The final set of discrete equations is given as [35][2]:

$$\frac{dN_i}{dt} = \sum_{\substack{j,k \\ x_{i-1} \le (x_j + x_k) \le x_{i+1}}}^{j \ge k} (1 - \frac{1}{2}\delta_{j,k})\eta\beta_{j,k}N_j\frac{N_k}{N_t} - N_i \sum_{k=1}^{M} \beta_{i,k}\frac{N_k}{N_t} \tag{2.23}$$

The first summation term on the RHS of Equation (2.23) represents the agglomeration into size interval i, with the representative size x_i. All combinations of particles that have a volume sum such that $x_{i-1} \le (x_j + x_k) \le x_{i+1}$ are considered. If $x_j + x_k = x_i$, η has the value 1. In other cases a fraction is computed:

$$\eta = \begin{cases} \frac{x_{i+1}-v}{x_{i+1}-x_i}, & x_i \le v \le x_{i+1} \\ \frac{v-x_{i-1}}{x_i-x_{i-1}}, & x_{i-1} \le v \le x_i \end{cases} \tag{2.24}$$

where $v = x_j + x_k$. $\beta_{j,k}$ is the coalescence kernel determining the rate of agglomeration. The Dirac delta function, $\delta_{j,k}$ makes sure that agglomeration events are not counted twice when $j = k$. The second term on the RHS of Equation (2.23) represents the rate of agglomeration out of the size interval i. M is the number of size intervals.

[2]The RHS of the equation has been divided by the total particle number, N_t because the coalescence kernel used here is defined differently than the coalescence kernel used in [35].

Chapter 3

Kinetic Modeling of Binary Agglomeration

3.1 Introduction

In this chapter, a new model framework for kinetic modeling of binary agglomeration is proposed. It results in a new population balance equation which must be solved numerically. An advantage of the new model framework is that it identifies three key terms of importance for the agglomeration kinetics. Each of these three terms represents a submodel. In the present work, two simple submodels are proposed and the third is taken from previous work found in the literature. Like existing models of binary agglomeration, this new model[1] cannot be used predictively because the model parameters are not known functions of material properties and operating conditions. It is emphasized that there is a potential in further work to develop better submodels that can be used predictively. This model framework encourages the start of such future work.

In Section 2.9.2 it was seen that the population balance equation for a batch system with binary agglomeration only, can be written:

$$\frac{\partial n(v)}{\partial t} = B_{\text{aggl}}(v) - D_{\text{aggl}}(v) \tag{3.1}$$

where the RHS are modeled using the coalescence kernel expressions,

$$B_{\text{aggl}}(v) = \frac{1}{2N_t}\int_0^v \beta(u, v-u)n(u)n(v-u)du \tag{3.2}$$

$$D_{\text{aggl}}(v) = \frac{1}{N_t}\int_0^\infty \beta(u, v)n(u)n(v)du \tag{3.3}$$

[1] The new model consists of the new model framework including the three submodels.

It was also pointed out that the above complicated continuous expressions have their counterpart in the much simpler discretized expression:

$$\frac{dN_i}{dt} = \beta_{j,k} N_j \frac{N_k}{N_t} \tag{3.4}$$

which describes the rate of change of particle number in size interval i due to agglomeration between particles in size intervals j and k. The continous Equation (3.1) with the expressions for the RHS given in Equations (3.2) and (3.3) can in fact be deduced from Equation (3.4). What this means, is that Equation (3.4), which has the advantage of being a simple expression, can be used as the basis for discussing the kinetics of binary agglomeration. There is no need to include the more complicated continuous description.

The new model framework, proposed in the next section, represents a new description of the binary agglomeration process. This means that a new equation is proposed to replace Equation (3.4). As discussed above, this new equation will also be used to deduce the continuous description.

3.2 New Model Framework

It is proposed that a general description of a binary agglomeration process includes three factors:

- The number of potential agglomeration events per unit time
- The probability of a potential agglomeration event involving two specific particle sizes
- The probability of successful agglomeration

Mathematically, this can be formulated:

$$\frac{dN_i}{dt} = \dot{N} p_{j,k} \alpha_{j,k} \tag{3.5}$$

The above equation represents a new description of the binary agglomeration process. It gives the rate of change of particle number in size interval i due to agglomeration between particles in size intervals j and k. $\dot{N}$ is the number of potential agglomeration events per unit time. Potential means that the agglomeration event may or may not be successful. $p_{j,k}$ is the probability of a potential agglomeration event involving particles from size intervals j and k. Only some fraction of the number of agglomeration events, will include the two size intervals j and k. $\alpha_{j,k}$ is the probability of successful agglomeration between the two particles from the mentioned size intervals. This new model framework is so general that it could be applied to any binary agglomeration process. It is simple, but it identifies three

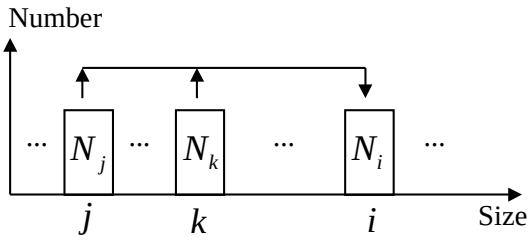

Figure 3.1: Particles from size intervals j and k agglomerating into the larger size interval i.

key areas of importance for the kinetics of binary agglomeration.

The continuous PBE can be deduced from Equation (3.5), and the result is the two expressions which replace Equations (3.2) and (3.3):

$$B_{\text{aggl}}(v) = \frac{1}{2}\int_0^v \dot{N}p(u, v-u)\alpha(u, v-u)du \tag{3.6}$$

$$D_{\text{aggl}}(v) = \int_0^\infty \dot{N}p(u, v)\alpha(u, v)du \tag{3.7}$$

where $p(u, v)$ and $\alpha(u, v)$ are the continuous counterparts of $p_{j,k}$ and $\alpha_{j,k}$, respectively. u and v are the volumes of the two particles agglomerating.

3.3 Modeling of $\dot{N}$

In case of FBG, the new model framework enables a new description of the agglomeration kinetics. Existing models all use the coalescence kernel, β in their model equations. As discussed in Section 2.9.2, β can be understood as a frequency of successful collisions. Very little is known about collision frequencies in granulation equipment, therefore the model parameter(s) in the expression for β must be fitted to experimental data. It is known that a collision can only be successful if surface liquid is present. Two surface dry particles cannot agglomerate. The coalescence kernel models miss this point as no information about the presence of surface liquid is included. These models only have a focus on collision frequencies. Because collisions between surface dry particles will not lead to agglomeration, this means that the collision frequencies (obtained after fitting of the model parameters) really are some kind of effective collision frequencies.

In this work, a potential agglomeration event is defined as collision with surface liquid available. It is proposed that the presence of surface liquid

is rate limiting and that collision frequencies are of secondary importance. FBG experiments generally show that a higher spray rate results in a higher rate of agglomeration. This would not be the case if the collision frequency was rate limiting and all particles were surface wet. Only a fraction of the particles in the fluidized bed are surface wet under normal operating conditions. If this was not the case, large, wet lumps of material would be formed by uncontrollable agglomeration—a situation referred to as *wet quenching* which is promoted by high spray rates and low bed temperatures. Even if the collision frequency is not rate limiting for agglomeration, the time between collisions will still influence the amount of surface liquid present at the time of collision and therefore influence the probability of successful collision.

The submodel for $\dot{N}$ given here will not involve any coalescence kernel at all. It will instead focus on the liquid available for potential agglomeration events. The following simple submodel is suggested:

$$\dot{N} = \frac{\dot{m}_{\text{spray}}}{m_{\text{event}}} \tag{3.8}$$

where $\dot{m}_{\text{spray}}$ is the liquid spray rate, and m_{event} is the liquid mass sprayed per potential agglomeration event. Assumptions of Equation (3.8) are:

- The supply of surface liquid is rate limiting
- The number of potential agglomeration events per unit time, $\dot{N}$ does not change during the granulation time (m_{event} has a constant value)

Equation (3.8) clearly links the number of potential agglomeration events per unit time to the spray rate. This is consistent with the assumption of the supply of surface liquid being rate limiting. There is, unfortunately, no way to estimate m_{event} a priori. It is, therefore, the first model parameter that must be fitted to experimental data.

The maximimum number of agglomeration events per unit time, $\dot{N}_{\max}$ can, however, be estimated. If it is assumed that each drop from the spray successfully results in an agglomerate, $\dot{N}_{\max}$ can be determined from knowledge of the spray rate and the drop size distribution (which can be measured with a laser diffraction instrument):

$$\dot{N}_{\max} = \dot{m}_{\text{spray}} \int_0^{x_{\max}} \frac{q_3(x)}{m_{\text{drop}}(x)} dx \tag{3.9}$$

where x denotes drop volume, and $q_3(x)$ is the mass density distribution. The expression $\int_{x_1}^{x_2} q_3(x)dx$ gives the mass fraction of the drop size distribution between sizes x_1 and x_2. $m_{\text{drop}}(x)$ is the mass of a drop with volume

x. Equation (3.9) makes it possible to determine a lower bound for m_{event}:

$$m_{\text{event,min}} = \frac{\dot{m}_{\text{spray}}}{\dot{N}_{\text{max}}} \tag{3.10}$$

If m_{event} is lower than this, $\dot{N}$ will be greater than $\dot{N}_{\text{max}}$, which is not possible with the assumptions made. This means that the exact value of the first model parameter is unknown, but it must be above a minimum value. The fact that the lower bound can be estimated, represents an improvement over the coalescence kernel models, where no bounds on the model parameters related to the collision frequency can be estimated.

Figure 3.2 illustrates the relationship between $\dot{N}_{\text{max}}$ and $\dot{N}$. The lower value of $\dot{N}$ is caused by physical effects like drop coalescence, surface drying and spray drying. Not all potential agglomeration events will be successful, so $\dot{N}_{\text{succ}}$ is smaller than $\dot{N}$.

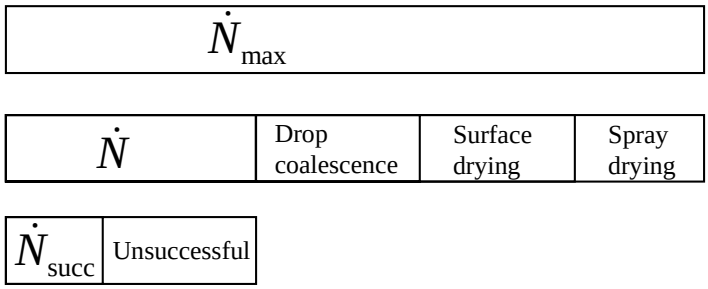

Figure 3.2: The figure indicates that $\dot{N}_{\text{succ}} \leq \dot{N} \leq \dot{N}_{\text{max}}$.

Coalescence of drops may happen in the spray and on the surfaces of the solid particles (illustrated in Figure 3.3). The residence time of a particle in the spray zone and the spraying conditions will determine the number of drops hitting it. If the mixing intensity is high, the solid particles spend a short time in the spray zone and may pick up few drops. In the opposite situation, the solid particles may pick up many drops. The spraying conditions are also important for drop coalescence. Schaafsma et al. [65] pointed out that the liquid distribution in the spray zone is determined by the ratio of the spray rate and the surface renewal rate (the supply rate of particles to the surface due to the bed's bubble-induced motion). Litster et al. [41] introduced a similar analysis for the description of the nucleation mechanism. A number called the *dimensionless spray flux* was proposed. Low values of this number indicate a low spray rate compared to the surface renewal rate, and therefore little coalescence of drops on particle surfaces.

Drying of liquid on particle surfaces is another effect reducing the number of potential agglomeration events. Figure 3.4 illustrates that a wetted particle may or may not be surface wet at the time of collision with another particle. If the particles in a collision are surface dry, it is not a potential agglomeration event according to the definition in this work. The bed temperature is very important for the drying rate, and the fluidization velocity will also be of influence. Let the drying time be defined as the time necessary for a particle to be surface dry after wetting, and let the collision time be defined as the time it takes before the particle collides with another particle after wetting. If the ratio of these two variables equals unity, it implies that the given particle is just surface dry at the time of collision. A ratio greater than one implies a surface wet particle at the time of collision because the drying time is greater than the collision time. The mentioned ratio is a random variable with some probability density function. Figure 3.5 illustrates that the fraction of wet particles that dry out before collision is given as an integral of the probability density function between the limits 0 and 1. It is, however, not known how to determine such a distribution.

Spray drying refers to solvent evaporation of the drops in the spray. The drops can be totally or partially evaporated as illustrated in Figure 3.6. The evaporation will increase as the distance between the nozzle and the bed surface is increased. A higher bed temperature and higher gas velocities will also increase the rate of spray drying.

There are many physical effects that determine $\dot{N}$. Many model variables describing physical behavior in a real FBG system follow unknown probability distributions. Examples of such model variables could be the liquid mass involved in an agglomeration event, the drying time of a particle, and the collision time. In this section, a simple submodel was proposed, which does not consider the complexities of the stochastic nature of the FBG process.

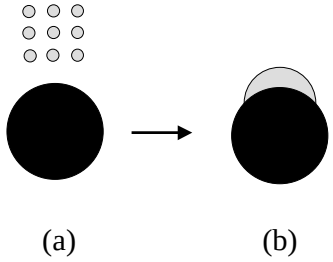

Figure 3.3: Drop coalescence. (a) Several drops from the spray hitting the same solid particle. (b) The drops coalesce on the particle surface.

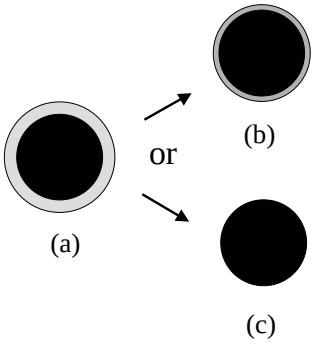

Figure 3.4: Surface drying. (a) Particle surrounded by a liquid layer. (b) Drying has caused a reduction in the liquid layer thickness. (c) The particle is completely surface dry.

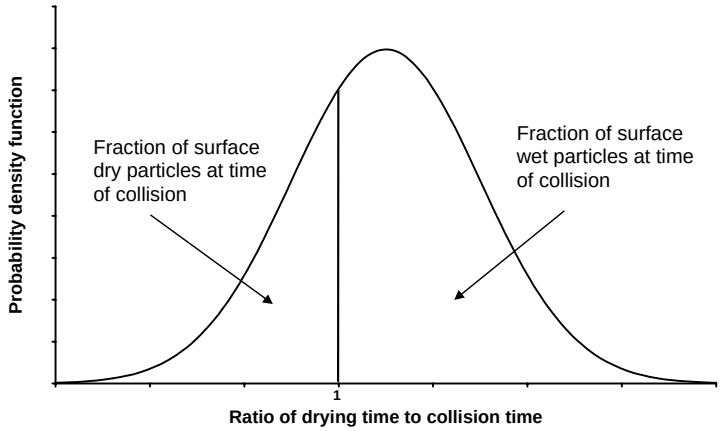

Figure 3.5: Probability distribution of the ratio of drying time to collision time.

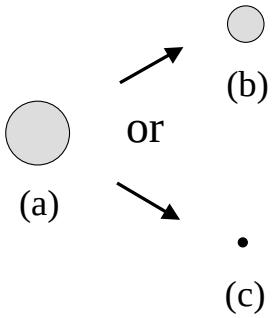

Figure 3.6: Spray drying. (a) Liquid drop. (b) Size of drop reduced due to drying. (c) Complete evaporation of solvent, only solute left.

3.4 Modeling of $p_{j,k}$

The probability of a potential agglomeration event involving particles from size intervals j and k, $p_{j,k}$ represents the second submodel. It can be understood as the fraction of agglomeration events per unit time involving particles from size intervals j and k. $\dot{N}p_{j,k}$ then becomes the number of agglomeration events per unit time involving particles from size intervals j and k.

In this section, a simple submodel for $p_{j,k}$ is proposed. The following assumptions are made:

- A potential agglomeration event consists of two steps: (1) Wetting of the particle in size interval j, and (2) Collision between the wetted particle and the dry particle in size interval k
- The probability of step one involving a particle in size interval j is equal to the area fraction of the particles in size interval j
- The probability of step two involving a particle in size interval k is equal to the area fraction of the particles in size interval k

Figure 3.7 can be used to explain the above assumptions. In step one, a liquid drop hits the first particle in size interval j. The area fraction of particles in size interval j is the sum of surface area of particles in size interval j divided by the total surface area in the bed. This fraction is also equal to the fraction of projected area. The probability of a drop hitting a solid particle in size interval j (step one) is modeled as the fraction of projected area of size interval j. This means that both the number and size of the solid particles influence the probability. In step two, the wetted particle in size interval j collides with another particle in size interval k. This probability is also modeled using the area fraction. Assuming the liquid drop has not spread out to make a film around the surface of the first particle, the size of the other particle will influence the probability of the liquid being present in the area of contact.

Using mathematical notation the above description becomes:

$$p_{j,k} = \begin{cases} f_{\mathrm{a},j} f_{\mathrm{a},k} + f_{\mathrm{a},k} f_{\mathrm{a},j} & \text{if} \quad j \neq k \\ f_{\mathrm{a},j} f_{\mathrm{a},j} & \text{if} \quad j = k \end{cases} \tag{3.11}$$

where $f_{\mathrm{a},j}$ is the area fraction of particles in size interval j, and $f_{\mathrm{a},k}$ is the area fraction of particles in size interval k. When $j \neq k$, the two-step process can take place in two different ways (first j then k, or first k then j), therefore the expression for $p_{j,k}$ becomes a sum.

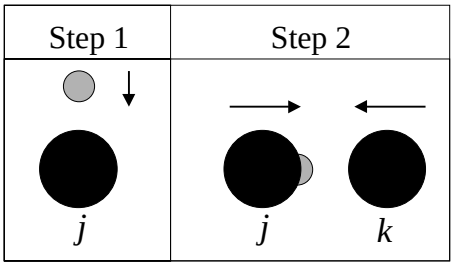

Figure 3.7: Modeling a potential agglomeration event as two-step process.

A simple example is used to explain the above equation: Imagine a small bed of particles consisting of 1000 solid spheres of diameter 100 μm and 1000 spheres of diameter 200 μm. This means that only two size intervals are needed to describe the population of particles. Because there are 1000 particles in both size interval number 1 and 2, the number fraction of both size intervals is 0.5. This can be seen in Table 3.1 which also shows the calculation of the area fraction of particles in each of the two size intervals. The area fraction of the particles in size interval 1, $f_{\mathrm{a},1}$ is 0.20, and the area fraction of the particles in size interval 2, $f_{\mathrm{a},2}$ is 0.80. Now that the area fractions are known, Equation (3.11) can be used to calculate $p_{1,1}$, $p_{1,2}$, and $p_{2,2}$. One obtains $p_{1,1} = 0.20 \cdot 0.20 = 0.04$, $p_{1,2} = 0.20 \cdot 0.80 + 0.80 \cdot 0.20 = 0.32$, and $p_{2,2} = 0.80 \cdot 0.80 = 0.64$. The sum of these three probabilities equals unity as they should. It is important to be aware of the fact that $p_{2,1}$ is just another way to write $p_{1,2}$, and that the two expressions are equal by definition. In general, $p_{j,k} = p_{k,j}$, just as the coalescence kernel, $\beta_{j,k} = \beta_{k,j}$. In numerical methods one avoids double use of these expressions by demanding e.g. $j \geq k$ (see Equation (2.23)).

3.5 Modeling of $\alpha_{j,k}$

The probability of successful agglomeration, $\alpha_{j,k}$ will be modeled here using the empirical expression used by Adetayo and Ennis [1, 2]. As discussed in Section 2.9.3, they defined an effective average particle volume, W to determine if a collision between two particles would lead to successful agglomeration or not:

$$W = \frac{(uv)^b}{(u+v)^{2b-1}} \tag{3.12}$$

where u and v are the two particle volumes, and b is a model parameter. If $W \leq W^*$ the collision is successful, while if $W > W^*$ it is unsuccessful. W^* is another model parameter.

Size interval, i	1	2
Particle diameter, d_i [m]	1.00E-04	2.00E-04
Particle number, N_i	1000	1000
Total particle number, N_t	2000	2000
Number fraction, $f_{n,i}$	0.5	0.5
Surface area, $N_i \pi d_i^2$ [m^2]	3.14E-05	1.26E-04
Total surface area [m^2]	1.57E-04	1.57E-04
Area fraction, $f_{a,i}$	0.20	0.80

Table 3.1: Constructed example to explain Equation (3.11).

In this work, the effective average particle mass, M is defined analogously:

$$M = \frac{[(\rho u)(\rho v)]^b}{[(\rho u) + (\rho v)]^{2b-1}} = \rho \frac{(uv)^b}{(u+v)^{2b-1}} \tag{3.13}$$

and will be used instead of Equation (3.12). The only difference is that mass is used instead of volume, because it is believed that this will result in a more general expression for M when materials with different densities are considered in different experiments[2]. This is an assumption that should be further investigated in the future. In discretized form, $M_{j,k}$ is then defined:

$$M_{j,k} = \frac{[(\rho x_j)(\rho x_k)]^b}{[(\rho x_j) + (\rho x_k)]^{2b-1}} = \frac{(m_j m_k)^b}{(m_j + m_k)^{2b-1}} \tag{3.14}$$

The submodel for $\alpha_{j,k}$ becomes:

$$\alpha_{j,k} = \begin{cases} 1 & \text{if} \quad M_{j,k} \leq M^* \\ 0 & \text{if} \quad M_{j,k} > M^* \end{cases} \tag{3.15}$$

where M^* is the critical effective average particle mass. Equation (3.15) is illustrated in Figure 3.8.

The concept of a critical effective average particle mass, M^* is further explained in Figure 3.9. Each of the contour lines shown corresponds to a certain b-value. All curves pass through the same point (m^*, m^*), where m^* is defined as the largest mass of a particle capable of successful agglomeration with another particle of equal size. For a given b-value, only

[2]For each experiment the density of the solid material is normally the same (except for the layered material from the spray), because the initial bed mass is of the same material.

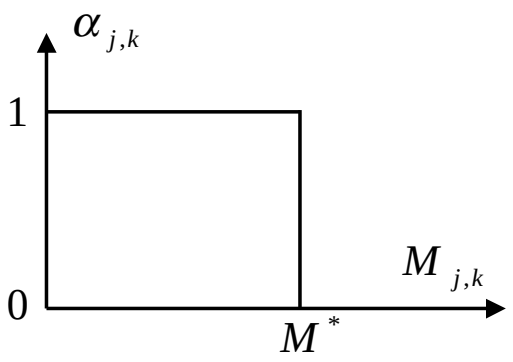

Figure 3.8: If the effective average particle mass $M_{j,k}$ is below a critical value, all potential agglomeration events are modeled as successful.

one contour line will pass through the point (m^*, m^*). This line represents the distinction between successful and unsuccessful agglomeration. Successful agglomeration takes place on the side of the line given by the point $(m^* - \delta, m^* - \delta)$, while agglomeration is unsuccessful on the side given by the point $(m^* + \delta, m^* + \delta)$. It can be seen that the shape of the critical contour lines in the figure is determined by the parameter b which may be interpreted as a parameter determining how easily other particle combinations than small-small can successfully agglomerate. Higher b-values increase the region in the figure where agglomeration is successful.

Using the definition of m^*, there is a connection between M^*, m^*, and b which can be found by setting $M_{j,k} = M^*$ and $m_j = m_k = m^*$:

$$\frac{(m^* m^*)^b}{(m^* + m^*)^{(2b-1)}} = 2^{(1-2b)} m^* = M^* \tag{3.16}$$

The significance of the above relation, is that one now has the choice of using either M^* or m^* as the third model parameter. In the next chapter, the use of m^* is chosen because of its easier interpretation. It is straightforward to show that $W^* = 2^{(1-2b)} w^*$, in case of the model of Adetayo and Ennis where the effective average particle volume is being used. The contour lines shown in Figure 3.9, represent different values of M^* which can be calculated using Equation (3.16). In the figure it can be seen that $m^* = 10^{-7}$kg in this example.

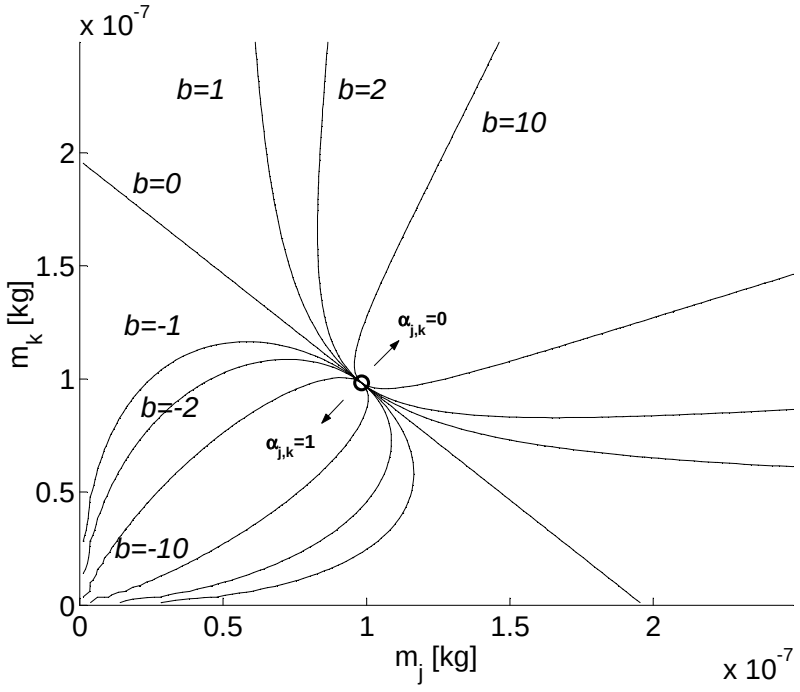

Figure 3.9: Contour lines shown for different b-values of the effective average particle mass function, $M_{j,k}$. These lines represent the distinction between the regions of unsuccessful and successful agglomeration. All lines pass through the point (m^*, m^*).

3.5.1 A Qualitative Theory for $\alpha_{j,k}$

Here, a qualitative analysis of a potential agglomeration event on the particle level is given. On initial contact between particles and liquid (initial agglomerate), the volume of that surface liquid compared to the particle volume will be very important for the successful formation of an agglomerate. The liquid causes capillary and viscous attractive forces to act between particles, and therefore acts like a glue. On the other hand, separating forces act on the initial agglomerate due to collisions with other particles or walls.

For future reference, V is loosely defined here as the ratio of the initial liquid volume binding the particles and some mean particle size. Figure 3.10 shows what initial agglomerates might look like for different V-ratios. For a given system, it seems very likely that the value of V will determine the growth mechanism and if successful agglomeration can occur. A high

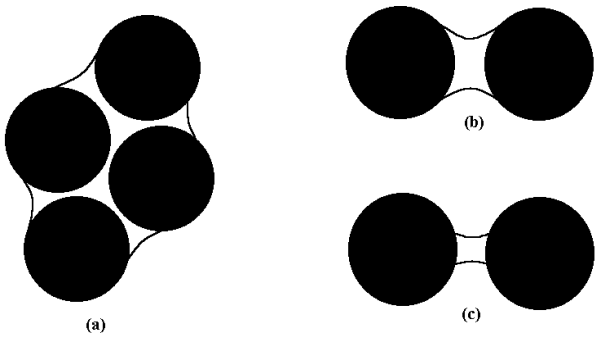

Figure 3.10: Initial agglomerates held together by liquid. (a) High V-value (b) Medium V-value (c) Low V-value.

value of V means that nucleation will be the main growth mechanism. In an intermediate range of V-values there will be sufficient liquid present to form a liquid bridge of sufficient strength between two particles. A low value of V means that the liquid bridge, if formed at all, will be too weak to withstand the subsequent separating forces acting on the agglomerate, and layering will be the major growth mechanism.

It is argued that the V-values and their distribution will determine the fraction of successful agglomeration events. A potential agglomeration event will be successful if the V-value is above a critical value. V can be understood as a ratio of attractive to separating forces. The critical V-value will be different in another system, with its set of material properties and process parameters. For example, in a system where a liquid with higher binder concentration (more viscous) is used, it seems likely that less liquid is needed to build a liquid bridge of equal strength (due to the increased viscous force), which means a lower critical value of V.

This qualitative analysis could be formulated mathematically. Assuming that the initial liquid volume, which could be defined as the volume of surface liquid present on the two particles in the moment they touch, is equal in all potential agglomeration events and that W in Equation (3.12) is used as the measure of the mean particle size, it is easy to show that the criterion of "the V-value being greater than a critical value" is equivalent to $W \leq W^*$. The conclusion is that the qualitative theory in this section is compatible with the empirical model of Adetayo and Ennis described in the last section.

3.6 Summary of the Model Framework with Submodels

3.6.1 Discretized Form

Model Framework:

$$\frac{dN_i}{dt} = \dot{N} p_{j,k} \alpha_{j,k} \tag{3.17}$$

Submodels:

$$\dot{N} = \frac{\dot{m}_{\text{spray}}}{m_{\text{event}}} \tag{3.18}$$

$$p_{j,k} = \begin{cases} 2 f_{\text{a},j} f_{\text{a},k} & \text{if} \quad j \neq k \\ f_{\text{a},j} f_{\text{a},j} & \text{if} \quad j = k \end{cases} \tag{3.19}$$

$$\alpha_{j,k} = \begin{cases} 1 & \text{if} \quad M_{j,k} \leq M^* = 2^{(1-2b)} m^* \\ 0 & \text{if} \quad M_{j,k} > M^* = 2^{(1-2b)} m^* \end{cases} \tag{3.20}$$

where,

$$M_{j,k} = \frac{(m_j m_k)^b}{(m_j + m_k)^{2b-1}} \tag{3.21}$$

Model Parameters:
The three model parameters are m_{event}, b, and M^* (or m^*).

3.6.2 Continuous Form

Model Framework:

$$\frac{\partial n(v)}{\partial t} = B_{\text{aggl}}(v) - D_{\text{aggl}}(v) \tag{3.22}$$

where,

$$B_{\text{aggl}}(v) = \frac{1}{2} \int_0^v \dot{N} p(u, v-u) \alpha(u, v-u) du \tag{3.23}$$

$$D_{\text{aggl}}(v) = \int_0^\infty \dot{N} p(u, v) \alpha(u, v) du \tag{3.24}$$

Submodels:

$$\dot{N} = \frac{\dot{m}_{\text{spray}}}{m_{\text{event}}} \tag{3.25}$$

$$p(u, v) = 2 f_{\text{a}}(u) f_{\text{a}}(v) \tag{3.26}$$

$$\alpha(u, v) = \begin{cases} 1 & \text{if} \quad M \leq M^* = 2^{(1-2b)} m^* \\ 0 & \text{if} \quad M > M^* = 2^{(1-2b)} m^* \end{cases} \tag{3.27}$$

where,

$$M = \rho \frac{(uv)^b}{(u+v)^{2b-1}} \tag{3.28}$$

Model Parameters:
The three model parameters are m_{event}, b, and M^* (or m^*).

3.7 Using the New Model Framework to Express a Coalescence Kernel Model

In this section, it is shown that the coalescence kernel model of Adetayo and Ennis [1, 2] discussed in Section 2.9.3 can be expressed using the new model framework. In their coalescence kernel model, all collisions are taken to be successful, as long as the average effective particle volume is below a critical value. According to Kapur and Fuerstenau [32], the size-independent coalescence kernel, β_0 used by Adetayo and Ennis (the symbol k is used in [32])represents the number of particles with which a given particle collides per unit time. Therefore, the number of potential agglomeration events per unit time is given by:

$$\dot{N} = \frac{\beta_0 N_{\text{t}}}{2} \tag{3.29}$$

where N_{t} is the total particle number, and it is divided by 2 so that collisions are not counted twice.

The birth rate (rate of change of particle number) in the larger size interval due to agglomeration between particles in size intervals j and k is [32]:

$$\beta_{j,k} N_j \frac{N_k}{N_{\text{t}}}$$

Because the agglomerating particles come from different size intervals, the death rates in size intervals j and k are equal the above expression. If two particles in the same size interval j agglomerate, the birth rate is (see for example [23, 35]):

$$\frac{1}{2} \beta_{j,j} N_j \frac{N_j}{N_{\text{t}}}$$

where the leading factor of 1/2 is included to avoid double counting. Because it takes two particles from size interval j to make one agglomerate, the death rate of particles in size interval j is equal to the above expression multiplied by two. The two above expressions can be summarized in the following form:

$$\frac{dN_i}{dt} = \begin{cases} \beta_{j,k} N_j \frac{N_k}{N_{\text{t}}} & \text{if} \quad j \neq k \\ \frac{1}{2} \beta_{j,j} N_j \frac{N_j}{N_{\text{t}}} & \text{if} \quad j = k \end{cases} \tag{3.30}$$

where i represents the size interval where the agglomerate is born. Combining Equations (3.17), (3.29), and (3.30) one can obtain:

$$p_{j,k}\alpha_{j,k} = \begin{cases} 2\frac{N_j}{N_t}\frac{N_k}{N_t}\frac{\beta_{j,k}}{\beta_0} & \text{if} \quad j \neq k \\ \frac{N_j}{N_t}\frac{N_j}{N_t}\frac{\beta_{j,j}}{\beta_0} & \text{if} \quad j = k \end{cases} \tag{3.31}$$

This last result can be split further into separate expressions for $p_{j,k}$ and $\alpha_{j,k}$:

$$p_{j,k} = \begin{cases} 2\frac{N_j}{N_t}\frac{N_k}{N_t} & \text{if} \quad j \neq k \\ \frac{N_j}{N_t}\frac{N_j}{N_t} & \text{if} \quad j = k \end{cases} \tag{3.32}$$

$$\alpha_{j,k} = \frac{\beta_{j,k}}{\beta_0} \tag{3.33}$$

Using Equation (2.20) in discretized form, the last equation can be rewritten:

$$\alpha_{j,k} = \begin{cases} 1 & \text{if} \quad W_{j,k} \leq W^* \\ 0 & \text{if} \quad W_{j,k} > W^* \end{cases} \tag{3.34}$$

Equations (3.29), (3.32), and (3.34) show that the coalescence kernel model of Adetayo and Ennis fits neatly into the new model framework. This result is very interesting, and it contributes to underscore the generality of the new model framework.

3.8 Numerical Method

The numerical discretization method of Kumar and Ramkrishna [35] was discussed in Section 2.9.4, and the final set of equations was:

$$\begin{aligned} \frac{dN_i}{dt} = & \sum_{\substack{j,k \\ x_{i-1} \leq (x_j + x_k) \leq x_{i+1}}}^{j \geq k} (1 - \frac{1}{2}\delta_{j,k})\eta\beta_{j,k}N_j\frac{N_k}{N_t} \\ & - N_i \sum_{k=1}^{M} \beta_{i,k}\frac{N_k}{N_t} \end{aligned} \tag{3.35}$$

where,

$$\eta = \begin{cases} \frac{x_{i+1}-v}{x_{i+1}-x_i}, & x_i \leq v \leq x_{i+1} \\ \frac{v-x_{i-1}}{x_i-x_{i-1}}, & x_{i-1} \leq v \leq x_i \end{cases} \tag{3.36}$$

and,

$$v = x_j + x_k \tag{3.37}$$

However, here the use of a coalescence kernel model is assumed. In order to use the new model framework, Equation (3.35) must be slightly modified. The result of this modification is the following equation:

$$\frac{dN_i}{dt} = \sum_{\substack{j,k \\ x_{i-1} \le (x_j + x_k) \le x_{i+1}}}^{j \ge k} \eta \dot{N} p_{j,k} \alpha_{j,k} - \sum_{k=1}^{M} (1 + \delta_{i,k}) \dot{N} p_{i,k} \alpha_{i,k} \tag{3.38}$$

where the new model framework has been introduced. The Kronecker delta, $\delta_{i,k}$ equals unity when $i = k$, and it makes sure that two particles are "used" for each agglomeration event when both particles in the event come from the same size interval. This is analogous to the factor of 1/2 used in the original equation to prevent collisions being counted twice. The important point is that when two particles in the same size interval agglomerate, two particles in that size interval die and one is born in a larger size interval. When particles from different size intervals agglomerate, one particle dies in each of those size intervals and one is born in a larger size interval.

One way to test the correctness of Equation (3.38) is to use Equations (3.29), (3.32), and (3.34) to substitute for $\dot{N}$, $p_{j,k}$, and $\alpha_{j,k}$, respectively. The original Equation (3.35) of Kumar and Ramkrishna is then obtained.

Chapter 4

Experimental Work

4.1 Introduction

The experimental work described in this chapter, was carried out during my stay as part of the group of Dr. Jim Litster at the Department of Chemical Engineering, University of Queensland, Australia. These experiments did not represent any distinct new development in themselves. The main goal was to obtain experimental data of the evolving PSD for comparison with the model developed in the last chapter. In addition, the experiments were very important for helping my physical understanding of the fluidized bed granulation process. The advantage of doing your own experiments is also that you know all the experimental conditions thouroughly, and there is no doubt how things were done.

This experimental work is concerned with agglomerate growth in a fluidized bed granulator. In order to better understand the agglomeration mechanism, larger initial solid particles (compared to the drop size) are used in most cases so that nucleation (one drop binding three or more particles in one event) probably will not occur. The growth mechanism of interest here is binary agglomeration. Layering will of course also take place, but the thin layers formed during an experiment do not contribute significantly to the increase in size.

For agglomeration to take place in the FBG process, the presence of a liquid is necessary. The liquid spray is often a solution, so that the bonds formed between particles solidify as the solvent evaporates in the drying air. The solid bonds formed can be very strong so that little breakage occurs (discussed in Section 4.3.6), and the formation of an agglomerate is then determined by the balance between attractive and separating forces until a final solid bond is established.

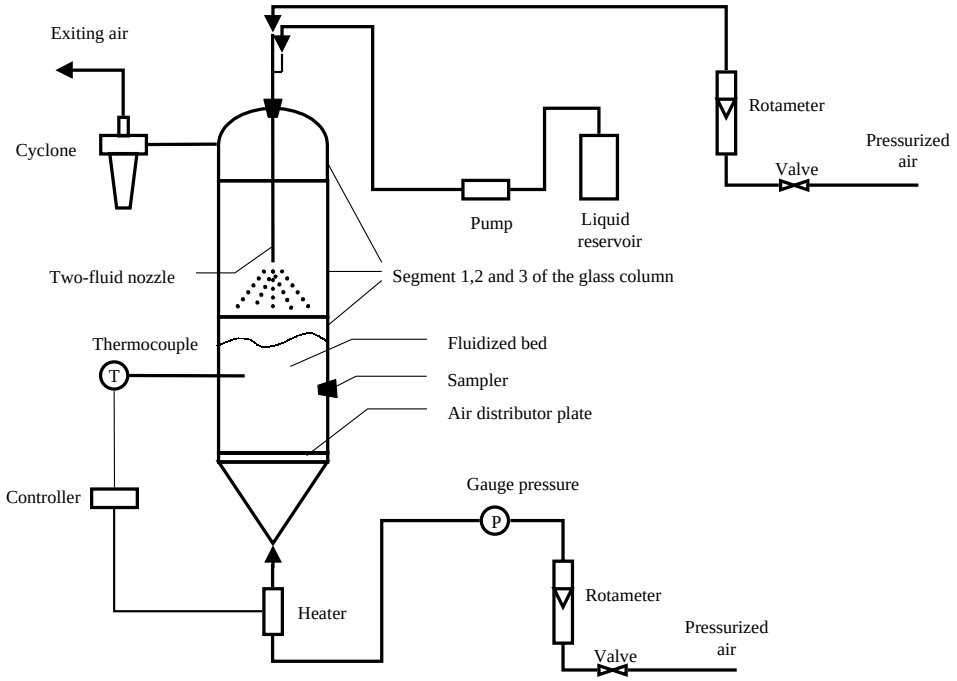

Figure 4.1: Schematic representation of the batch fluid bed granulator.

4.2 Experimental

4.2.1 Experimental Apparatus

Experiments were performed in a batch fluid bed granulator shown schematically in Figure 4.1. The glass column has an inner diameter of 15 cm. A heater element with capacity of 3 kW is used to heat up the inlet air, and a controller connected to a thermocouple in the bed keeps the temperature almost constant at the desired level. The liquid is top-sprayed on to the bed through a two-fluid nozzle (an airflow is used to atomize the liquid).

4.2.2 Particulate Material and Granulating Liquid

The particulate material used is specified in Table 4.1. The liquid chosen was a solution of polyvinylpyrrolidone (PVP), normally 0.04 g PVP/ g water. The molecular weight of the PVP was 360 K.

4.2.3 Procedure

In each run, the fluid bed was first filled up with a certain mass of solid particles. Then the fluidizing air was turned on. When the bed temperature had reached the chosen set point, the liquid spraying was started.

Lower sieve size [mm]	0.000	0.125	0.250	0.355	0.500	Mass mean
Upper sieve size [mm]	0.125	0.250	0.355	0.500	0.710	diameter[mm]
Sodium chloride [%]	0.0	1.5	13.9	78.3	6.3	0.42
Glass beads [%]	0.5	58.0	41.5	0.0	0.0	0.23

Table 4.1: Initial PSDs for sodium chloride and glass beads.

The nozzle was positioned 20 cm above the static bed surface. During an experiment the bed temperature was maintained steadily at the set temperature with a deviation of less than 1-2 degrees Celsius. The experiment was either run for a given time, or for a given amount of liquid sprayed. In some runs it was necessary to increase the superficial gas velocity, because of the increase in the minimum fluidization velocity due to the agglomerate growth and stickiness of the particles. Sometimes it is claimed in the literature [79, 14] that the excess gas velocity in a batch experiment is kept constant. This strategy was not chosen because the minimum fluidization velocity is unknown during an experiment. Therefore the excess gas velocity cannot be calculated beforehand. Rather than "keeping the excess gas velocity constant", the superficial gas velocity was adjusted in steps and logged. Table 4.2 summarizes all the experiments that were carried out.

Experiment number	Spray rate [g/min]	Nozzle air [g/min]	Bed temperature [deg. C]	Binder concentration [g PVP/ g H2O]	Initial bed mass [kg]	Particulate material	Liquid sprayed/ Duration [g] or [min]
E1	3.8	85	85	0.04	4.3	NaCl	60 min
E2	**12.9**	85	85	0.04	4.3	NaCl	2400 g
E3	**20.5**	85	85	0.04	4.3	NaCl	900 g
E4	4.0	**56**	85	0.04	4.3	NaCl	150 g
E5	4.0	85	**70**	0.04	4.3	NaCl	60 min
E6	4.1	85	**55**	0.04	4.3	NaCl	60 min
E7	4.2	85	85	**0.02**	4.3	NaCl	60 min
E8	4.0	85	85	**0.00**	4.3	NaCl	60 min
E9	12.7	85	85	0.04	**2.0**	NaCl	280 g
E10	4.2	85	85	0.04	**1.0**	NaCl	140 g
E11	13.0	85	85	0.04	4.6	**Glass beads**	1682 g

Table 4.2: Summary of the experiments carried out.

4.2.4 Sampling

A 10 mm opening with a rubber stopper in the glass column was located midway between the distributor and the bubbling surface. Samples were taken from the bed at certain intervals during each run by removing the stopper for a short time. The mass of each sample taken was normally

50-100 g, and more than 10 % of the total bed mass was never removed. Sieve analysis was used to determine the size distribution. Several tests were done to ensure that this method would give a good representation of the true PSD in the bed. Table 4.3 shows that the method of sampling gives a good estimate of the true PSD in the bed.

Size range [mm]	Sample [%]	"True" PSD [%]	Sample [%]	"True" PSD [%]	Sample [%]	"True" PSD [%]
0.000 - 0.250	0.43	0.44	0.11	0.14	0.78	0.65
0.250 - 0.355	5.24	5.26	1.63	1.78	7.44	7.18
0.355 - 0.500	38.63	37.58	17.93	17.78	47.99	47.52
0.500 - 0.710	42.47	40.31	32.05	28.77	37.81	36.99
0.710 - 1.000	13.24	16.41	46.98	49.50	5.98	7.66
1.000 - 1.180	0.00	0.00	1.30	2.03	0.00	0.00
Sum %	100.00	100.00	100.00	100.00	100.00	100.00
Mass mean dia.	0.55	0.56	0.69	0.70	0.51	0.51

Table 4.3: Comparison of the mass PSD obtained from sampling versus the PSD obtained by splitting of the entire bed content. Results from the experiments are shown.

4.2.5 Drop Size Measurements

The drop PSD was measured for most of the spraying conditions used. This was done with a Malvern 2600 laser diffraction instrument. The spray was measured with a horizontally positioned nozzle at room temperature, and the laser beam was located perpendicular to the nozzle (in the same plane) at a distance of 16 cm. The results of the measurements are summarized in Table 4.4. D_{10}, D_{50}, and D_{90} are the drop diameters, which below there is 10, 50 and 90 percent of the liquid volume, respectively.

Spray rate [g/min]	Nozzle air [g/min]	D_{10} [µm]	D_{50} [µm]	D_{90} [µm]
4	85	24	66	210
13	85	28	96	300
21	85	32	108	318

Table 4.4: Diameters characterizing the drop PSD at three different spray rates of PVP solution (0.04 g PVP/ g water).

4.3 Results and Discussion

Figure 4.2 shows some typical SEM images of agglomerates obtained from the fluidized bed. Initial single particles and final agglomerates are shown

for both sodium chloride and glass beads. The details of the experimental results at various conditions are presented below.

4.3.1 Effect of Spray Rate and Drop Size

To investigate the effect of liquid spray rate on the PSD, three different spray rates were chosen. Figure 4.3 shows a plot of the mass mean diameter versus the liquid sprayed (not time). The graph indicates clearly that a higher liquid spray rate gives more agglomeration per liquid sprayed. The same trend was found in [69]. Two possible reasons are: (1) The drop sizes are larger at a higher spray rate, and (2) the denser spray (shorter distance between drops) at a higher spray rate could lead to more drop coalescence. Both of these effects supply more liquid to an initial agglomerate, which means a higher value of V (see Section 3.5.1).

Since the effect of drop coalescence and drop size cannot be separated in the above experiments, further experiments were carried out on the effect of drop size by reducing the atomizing air while keeping the spray rate constant. Although the drop size at nozzle air rate of 56 g/min was not measured, it will be larger than that at 85 g/min due to the lower atomizing air pressure. The mass mean diameter against the total liquid sprayed is also shown in Figure 4.3 (E4). It is seen that the growth rate at larger drop sizes is higher than that at smaller drop sizes, indicating that drop size could be the main factor causing higher growth. A larger drop size in the spray will supply more liquid to the initial agglomerate, thereby increasing V. Further experiments need to be done to study the effect of spray rate on agglomeration when the drop sizes are kept constant.

4.3.2 Effect of Bed Temperature

Three experiments lasting for 60 minutes were done for different bed temperatures (55 °C, 70 °C and 85 °C). The influence of bed temperature on the mass mean diameter is shown in Figure 4.4. It can be seen that a higher bed temperature causes a lower rate of agglomerate growth. This is consistent with the results of Schaafsma et al. [65]. An increased rate of spray drying and faster drying of liquid on particle surfaces result in less liquid available for an initial agglomerate (reduced V-value). In addition, a higher temperature will lower the viscosity of the liquid, possibly resulting in weaker liquid bridges.

4.3.3 Effect of Binder Concentration

Three different binder concentrations of 0.00 (pure water), 0.02 and 0.04 (g PVP/ g water) were chosen. Figure 4.5 shows that a liquid with a higher binder concentration causes more rapid agglomeration. This was also found

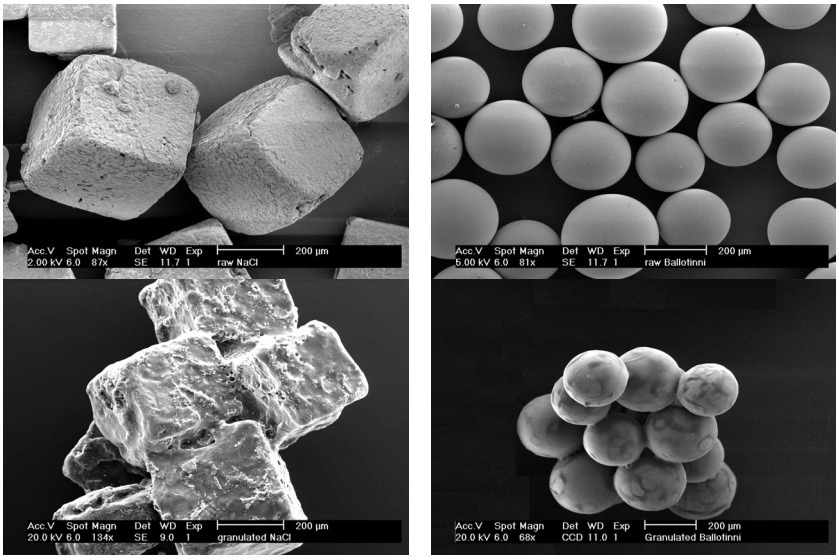

Figure 4.2: SEM pictures of the initial and agglomerated particles. Left: sodium chloride. Right: Glass beads.

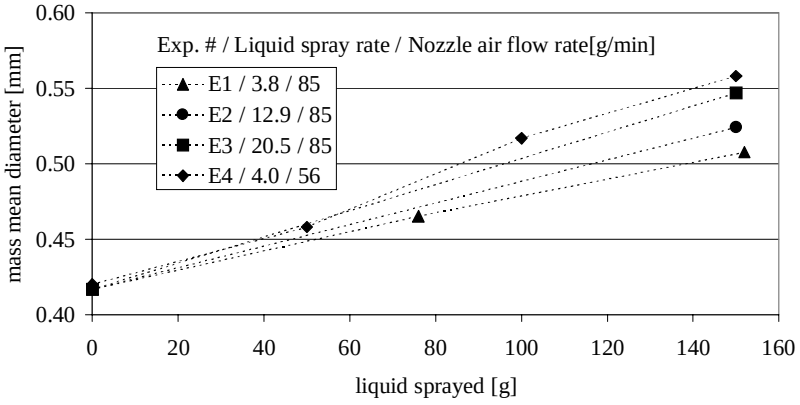

Figure 4.3: Mass mean diameter as a function of liquid sprayed for Experiments E1-E4 in Table 4.2. The fluidization velocity for the range shown is 0.5 m/s.

by Schaefer and Worts [70]. Possible explanations are: (1) The viscosity of the liquid will increase with higher binder concentration, thereby making the liquid bridges stronger so that an initial agglomerate can survive more separating forces, (2) the drop size is increased due to the higher viscosity, and (3) the more viscous liquid could dry more slowly. All of these effects cause either stronger liquid bridges (higher viscous forces) or more liquid available to an initial agglomerate (higher V-value). Note that pure water gives no agglomerate growth for this system. Even if the pure water could form an initial agglomerate because of capillary and viscous forces, there are not strong enough solid bonds after the water has evaporated.

4.3.4 Stages in Fluid Bed Agglomeration

Different stages of agglomerate growth can be observed in a long experiment. As the solids increase in size and the drops remain the same (V decreases), a slower growth seems more likely. A lower V-value is equivalent to an increase in the separating forces (for a given system).

An experiment spraying 2400 g of liquid was done to observe the growth in a longer run. It can be concluded from Figure 4.6 that the growth flattens off with time/liquid sprayed as expected. During the experiment, it was necessary to increase the gas to keep the solid particles fluidized. The gas velocity is also shown in the figure. The evolving PSD as a function of liquid sprayed is shown in Figure 4.7.

A similar experiment using smaller glass beads was also done, spraying 1682 g of liquid. At the end of the experiment it had to be stopped because of slugging fluidization. The mass mean diameter as a function of liquid sprayed is shown in Figure 4.8 and the evolving PSD is shown in Figure 4.9. This system shows no tendency to slower agglomerate growth, possibly due to the smaller initial solid particles.

4.3.5 Different Initial Bed Charges

Three experiments using bed charges of 1 kg, 2 kg and 4.3 kg were carried out. A ratio S is here defined as the mass of liquid sprayed divided by the initial bed charge/mass. In each case an amount of liquid was sprayed so that $S = 0.14$. From Fig. 4.10 it can be seen that the three curves show good agreement, indicating the importance of the S-ratio. However, it was found that a spray rate of 12.7 g/min resulted in wet quenching (overwetting of the bed surface resulting in uncontrollable agglomeration and defluidization) for the case with a bed charge of 1 kg, therefore a lower spray rate was used. To use S as an indication of the extent of the agglomerate growth, a certain solid surface area and particle mixing is

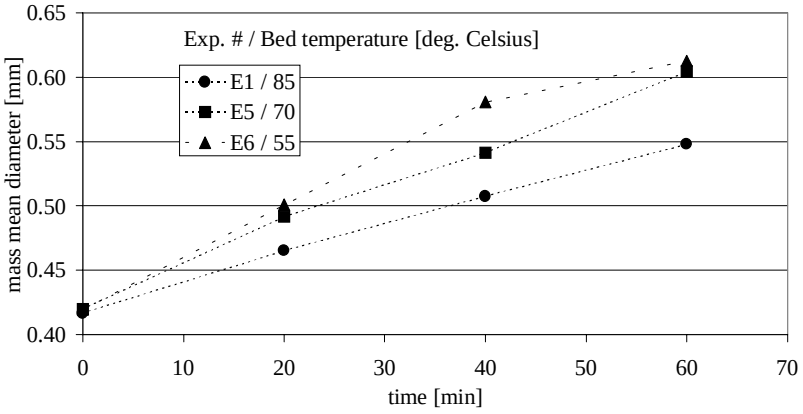

Figure 4.4: Mass mean diameter as a function of time for Experiments E1, E5, and E6 in Table 4.2. The fluidization velocity is 0.5 m/s.

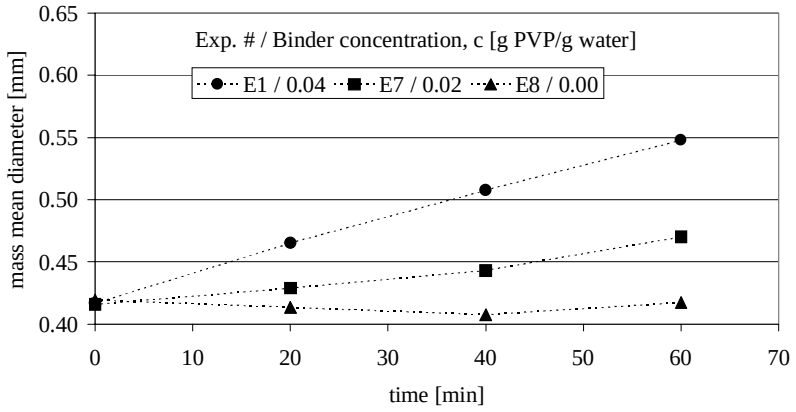

Figure 4.5: Mass mean diameter as a function of time for Experiments E1, E7, and E8 in Table 4.2. The fluidization velocity is 0.5 m/s.

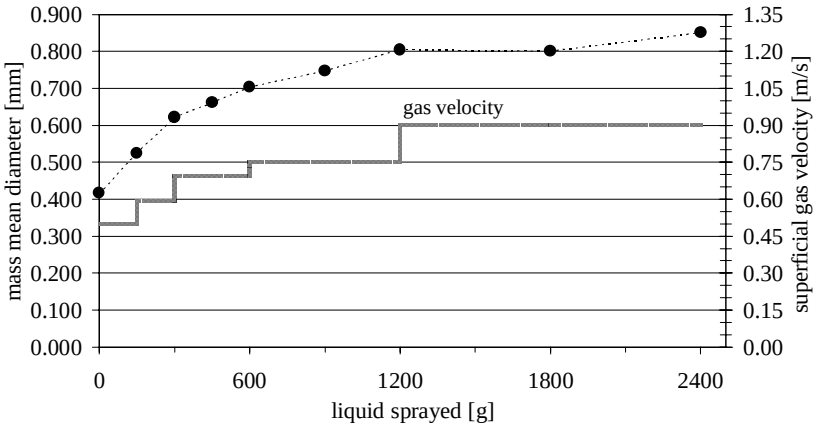

Figure 4.6: Mass mean diameter as a function of liquid sprayed. Also shown is the gas velocity, U. This is Experiment E2 in Table 4.2.

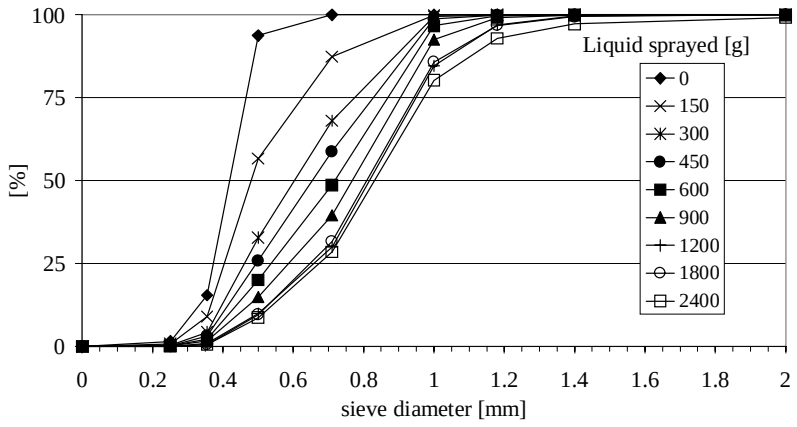

Figure 4.7: The mass cumulative undersize distribution for different amounts of liquid sprayed. Same experiment as in Figure 4.6.

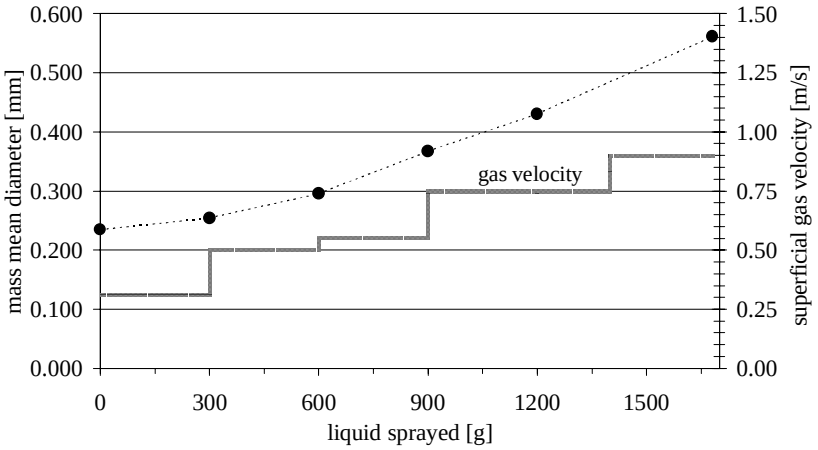

Figure 4.8: Mass mean diameter as a function of liquid sprayed. Also shown is the gas velocity, U. This is Experiment E11 in Table 4.2.

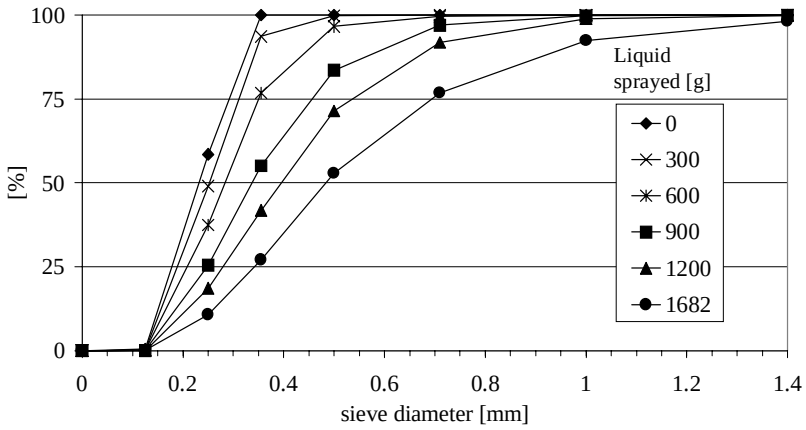

Figure 4.9: The evolving mass cumulative undersize distribution for different amounts of liquid sprayed. Same experiment as in Figure 4.8.

necessary to avoid wet quenching for a given spray rate.

4.3.6 Breakage and Attrition

An experiment was done to investigate the breakage and attrition of agglomerates. Spraying was turned off after granulating for 60 minutes, and then running for additional 60 minutes with the same gas velocity and bed temperature. Figure 4.11 shows how the mass fraction in each size interval changes with time. The main conclusion that can be drawn from the graph is that little breakage and attrition occur. Except for the data point at 80 minutes, the curves principally level off. However, some loss seems to be the trend for the largest size fraction. This could be due to the higher separating forces probably acting on larger agglomerates in a fluid bed.

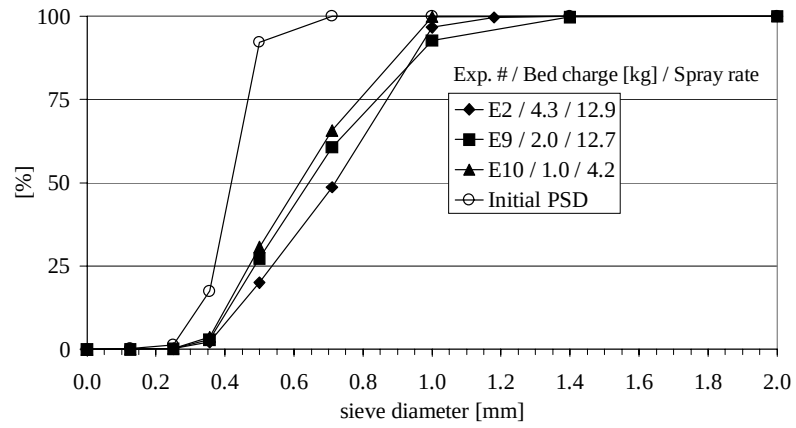

Figure 4.10: The mass cumulative undersize distribution for three different initial bed charges, but same ratio of liquid sprayed to bed charge, $S = 0.14$ The experiments shown correspond to Experiments E2, E9 and E10 in Table 4.2.

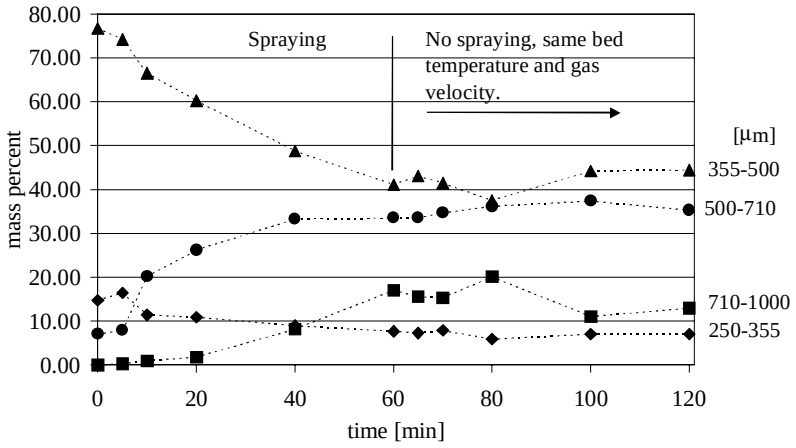

Figure 4.11: Mass percent in each size fraction as a function of time. This experiment is a continuation of Experiment E1. Spraying is stopped and the particles are agitated and heated under the same conditions for an additional 60 minutes.

4.4 Conclusions

For two particles to agglomerate, liquid has to be present to form a liquid bridge, which also must have sufficient strength. Effects that sustain the presence of liquid and its ability to form strong liquid bridges will lead to more agglomeration. The V-ratio, here loosely defined as the ratio of the initial liquid volume binding the particles and some mean particle size, is one important factor in the proposed qualitative theory of agglomeration kinetics. Higher V-values are achieved by lowering the bed temperature, lowering the amount of nozzle air (larger drops), and result in a higher fraction of successful agglomeration events. Things are complicated a little bit by the fact that the number of potential agglomeration events per unit time, $\dot{N}$ also is important for the growth rate. For example, a larger drop size will increase V, but $\dot{N}$ is reduced. Therefore, it is not obvious what the effect on growth rate will be. However, the experiments carried out show that the increase in V more than compensates for the reduction in $\dot{N}$. Increasing the binder concentration has to effects (1) the critical V-value is reduced because of the stronger liquid binder (2) the V-values are increased due to bigger spray drops. A higher spray rate gives more agglomerate growth per liquid sprayed, possibly caused by a larger drop size and more drop coalescence, which both increase V.

Different stages in the batch agglomeration process can exist. A changing balance between the attractive and separating forces acting on an newly formed agglomerate explains this. As the particle size increases (and the gas velocity often is increased to keep the solids fluidized), the separating forces caused by collisions are also increased. The attractive forces will, at some point, be too small to hold the initial agglomerate together, due to insufficient presence of liquid. This evolution may be expressed as a gradual decrease in V. The V-ratio is an indication of the balance between attractive and separating forces acting on an initial agglomerate. The different growth stages of agglomerate growth (nucleation, "agglomeration" and coating) can all be explained by a gradual decrease in V (see Figure 3.10). The above analysis qualitatively agrees with the granulation regimes suggested by Ennis et al. [14], but has a focus on the presence of surface liquid instead of collisional velocities.

The ratio of liquid mass sprayed and initial bed mass, S gives a good indication of the extent of agglomeration. However, if the initial bed mass is too small, S is no longer a good indication because overwetting of the bed results in wet quenching.

Little breakage and attrition was observed in the granulation of sodium chloride. This means that important effects controlling agglomeration are

wetting, drying, formation of liquid bridges, and their dynamic strengthening, not the rate of breakage and attrition.

Chapter 5

Simulation and Fitting of Model Parameters

5.1 Introduction

This chapter deals with simulation of the evolving PSD using the new population balance model which consists of the new model framework including the three submodels (summarized in Section 3.6). Some challenges in comparing simulation results with experimental FBG data are discussed. The new model is compared that of Adetayo and Ennis which is considered to be the state-of-the-art model, and some fundamental differences are pointed out. Finally, the experiments described in Chapter 4 are used to estimate the values of the model parameters under different conditions.

The computer code *pop_balance* was written in Fortran 90 to solve the population balance equation. It uses the numerical method of Kumar and Ramkrishna described earlier. The subroutine *nag_rk_step* from NAG which is a Runge-Kutta method for solving an initial value problem for a system of first order ordinary differential equations has been applied. Both the new model and the model of Adetayo and Ennis are programmed. The code can handle simultaneous growth by layering and binary agglomeration very well, but this has not been focused on in this work. As the initial condition for the PSD, a standard normal distribution can be chosen, or a PSD obtained from sieve analysis can be read from file and converted to a continuous distribution by interpolation. The numerical grid used is described in [42], and its fineness can be adjusted by a parameter.

Figure 5.1 is an example of how the results from a simulation will be presented. The computed PSDs are shown for different times of the simulation. To the left is the initial PSD ($t = 0$), which is used as the initial condition for the calculation. A PSD is represented as a plot of the cumulative mass

fraction versus the volume diameter of a particle. The volume diameter is defined as the diameter of a perfect sphere with the same volume as the actual particle. This is the obvious choice because the population balance framework conserves the volume of the two particles in an agglomeration event. No information on the particle structure is stored.

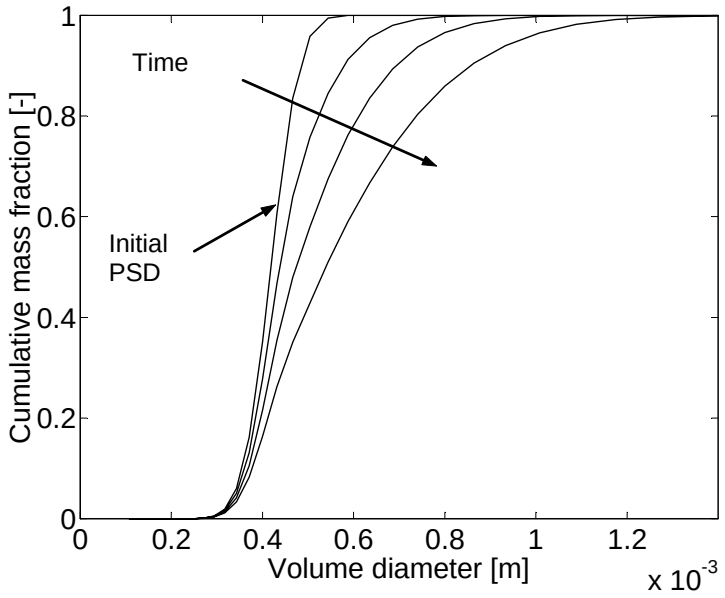

Figure 5.1: A typical plot to present the simulation result of how the PSD changes as a function of time. The PSD furthest to the left is the initial PSD.

5.2 Challenges in Comparing Simulation Results with Experimental Data

There are a few major challenges when comparing the PSDs from a simulation with experimentally obtained PSDs. As discussed in the previuous section, the calculculated PSDs are represented by plots of the cumulative mass fraction versus the volume diameter. However, the most common method of particle size analysis in FBG is sieving. The PSD obtained by experiments is therefore represented by a plot of the cumulative mass fraction versus the sieve diameter. A conversion from sieve diameter to volume diameter is therefore neccessary. Waldie et al. [88] pointed out that this conversion is not straightforward. For one size fraction the sieve diameter, $\bar{d}$ can be defined as the average aperture of the two sieves. The mass of a sphere with a diameter equal to the sieve diameter is then $\rho\pi\bar{d}^3/6$. By

counting and weighing a large number of particles in a size fraction, the average particle mass can be calculated as m/N. Waldie et al. defined the apparent fractional voidage as follows:

$$\epsilon_{\text{app}} = \frac{m/N}{\rho\pi\bar{d}^3/6} \tag{5.1}$$

This number was shown to vary with particle size and will be dependent upon many factors, so no simple rule can be used. For larger, porous agglomerates in FBG this voidage will be less than one. However, for the initial sodium chloride particles used in the experiments described earlier, it seems very likely that this voidage would be greater than one. This can be explained by the cubical geometry of these particles.

Another difficulty is related to the assumption that the growth mechanism actually taking place is only binary agglomeration. This is assumed in the population balance model. If other growth mechansims actually occurred in the experiments and played a major role, it would of course be meaningless to compare model predictions with experimental data. There is no strict guarantee that nucleation could not take place for example, even though the drop size used was small compared to the initial particles. Some breakage could also represent a problem. Layering and attrition will probably not be a source of error because these processes are slow compared to the growth by agglomeration.

Because of these challenges, the comparison of simulation results with experimental data is not as exact as one could wish. For this reason, no effort has been put into statistical analysis of the values of the model parameters. The emphasis has been to point out the principal effect of changed material properties and operating conditions on the model parameters.

5.3 The New and the Old Model

It was shown in Section 3.7 that the coalescence kernel model of Adetayo and Ennis [1, 2] fits into the new model framework. Their model is now referred to as the old model. The new and the old model have different submodels, which result in different simulation results under similar conditions. Figure 5.2 shows the results from simulations with both the new and the old model. The initial PSD and the simulation time were identical in the two cases. Large values of m^* and w^* were chosen so that $\alpha_{j,k}$ would always be equal to one which means all potential agglomeration events were considered successful. The observed differences in the figure must therefore have to do with the different submodels for $\dot{N}$ and $p_{j,k}$. It is clear that the PSD evolves much faster when the new model is used.

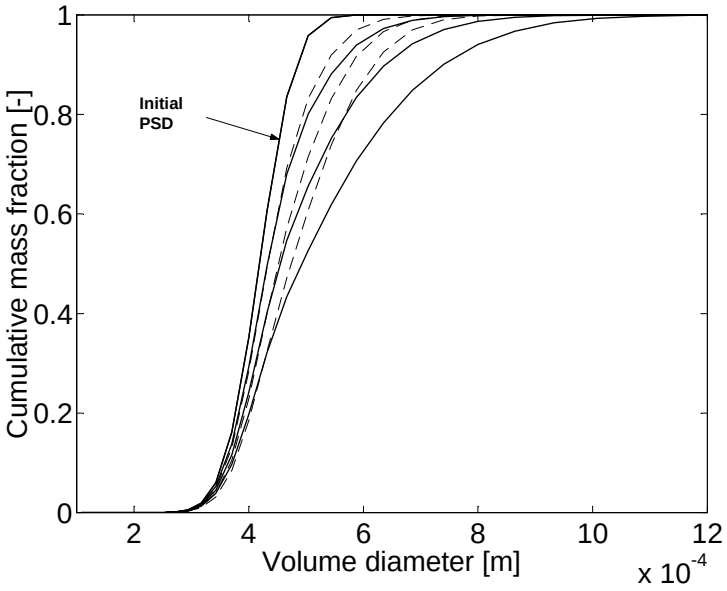

Figure 5.2: Results from simulations with both the new model (solid lines) and the old model (dashed lines).

The number of potential agglomeration events per unit time, $\dot{N}$ has been modeled differently. In the new model the following submodel is used (see Equation (3.8)):

$$\dot{N} = \frac{\dot{m}_{\text{spray}}}{m_{\text{event}}} \tag{5.2}$$

while the old model uses the submodel (see Equation (3.29)):

$$\dot{N} = \frac{\beta_0 N_{\text{t}}}{2} \tag{5.3}$$

The two above expressions are fundamentally different, the first expression is derived from the theory that the presence of surface liquid is rate limiting, and $\dot{N}$ is constant, while the second expression is derived from the theory that collisions are rate limiting, and $\dot{N}$ is decreasing as N_{t} is reduced during the process. In the simulations presented in Figure 5.2, the values of the model parameters m_{event} and β_0 have been chosen so that $\dot{N}$ has the same value at the start of the simulation. One explaination of the slower evolution of the PSD when the old model is used, is therefore, the gradual decrease in $\dot{N}$ which is not the case when the new model is used. In Figure 5.3, $\dot{N}$ is shown as a function of time for the simulations presented in Figure 5.2.

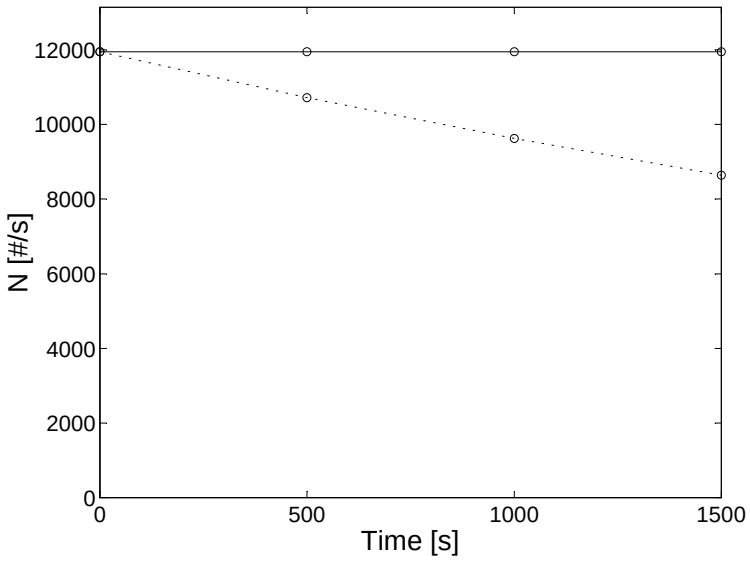

Figure 5.3: Plot of $\dot{N}$ as a function of time for the new model (solid line) and for the old model (dotted line).

The probability of a potential agglomeration event involving particles from size intervals j and k, $p_{j,k}$ has also been modeled differently. While the new model uses the submodel (see Equation (3.11)):

$$p_{j,k} = \begin{cases} 2f_{\mathrm{a},j}f_{\mathrm{a},k} & \text{if} \quad j \neq k \\ f_{\mathrm{a},j}f_{\mathrm{a},j} & \text{if} \quad j = k \end{cases} \tag{5.4}$$

the old model uses the submodel (see Equation (3.32)):

$$p_{j,k} = \begin{cases} 2\frac{N_j}{N_\mathrm{t}}\frac{N_k}{N_\mathrm{t}} & \text{if} \quad j \neq k \\ \frac{N_j}{N_\mathrm{t}}\frac{N_j}{N_\mathrm{t}} & \text{if} \quad j = k \end{cases} \tag{5.5}$$

These two submodels are very similar in their form. In Section 3.4 it was assumed that a potential agglomeration event consisted of two steps. Step one was the wetting of a particle. Step two was collision between the wetted particle and a dry particle. The probability of each step involving a particle from a certain size interval was modeled using the area fraction. If instead the number fraction had been used, one would in fact obtain Equation (5.5). The use of area fraction instead of number fraction favors the coalescence of large particles compared to small particles. This is now explained. Figure 5.4 shows the number and area fractions of the initial PSD in Figure 5.2 as a function of size interval. It can be seen that the

area fraction curve is shifted to the right compared to the number fraction curve. For the same j and k, Equation (5.4) will therefore result in a higher value for $p_{j,k}$ than Equation (5.5) which means that coalescence of larger particles is favored using the new model. This is another explanation of the differences observed in Figure 5.2.

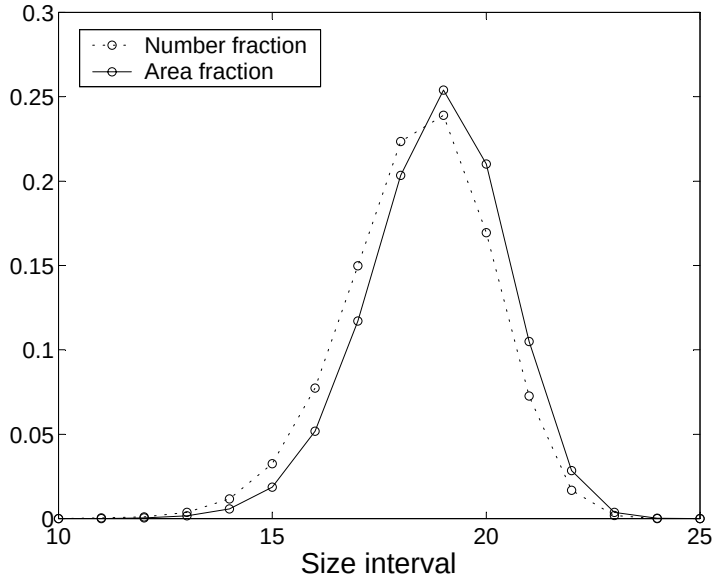

Figure 5.4: Plot of the number and area fractions as a function of size interval for the initial PSD used in Figure 5.2.

It has now been demonstrated that the two models predict different PSDs under similar conditions. However, in real experiments it cannot generally be assumed that all $\alpha_{j,k} = 1$. This makes the situation more complicated. Using both the new and the old model to simulate experiment E2 in Table 4.2 on p. 47, it was shown that both the new and the old model are able to fit the experimental data fairly well by adjusting the three model parameters. This can be seen in Figure 5.5 and in Figure 5.6. The implication of this result is that experimental growth curves (PSDs at time intervals) cannot easily be used to verify the submodels of the general model framework. Differences in the two first submodels ($\dot{N}$ and $p_{j,k}$) pointed out may be compensated by other differences in the last submodel ($\alpha_{j,k}$) in such a way that the overall results are very similar as shown in the two figures. It is not claimed that the new model is better than the old one in fitting the experimental data.

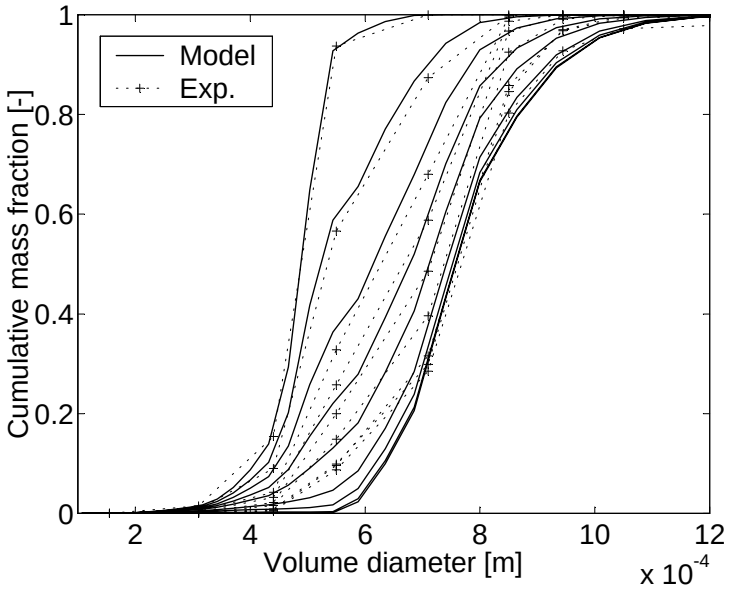

Figure 5.5: Simulation using the new model. The model parameters used are $m_{\text{event}} = 1.8 \cdot 10^{-8}$ kg, $m^* = 2.15 \cdot 10^{-7}$ kg, and $b = 1.5$.

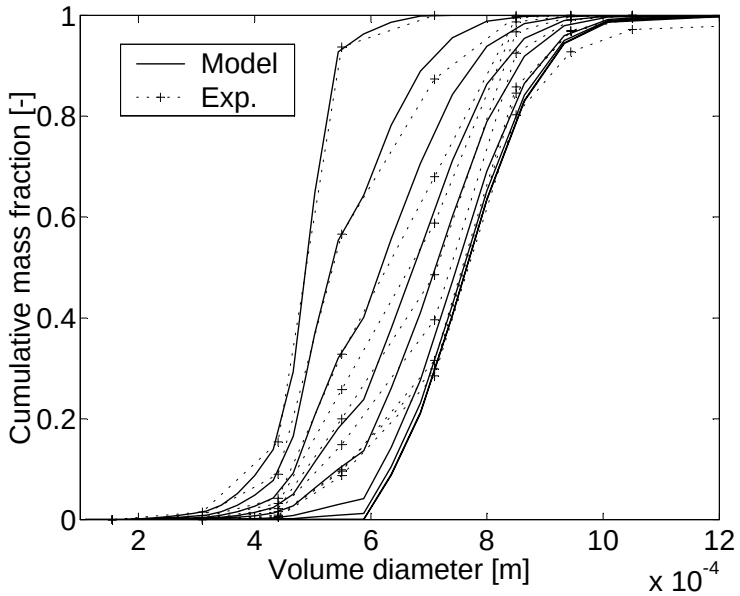

Figure 5.6: Simulation using the old model. The model parameters used are $\beta_0 = 0.9 \cdot 10^{-3}$ s^{-1}, $w^* = 1.16 \cdot 10^{-10}$ m^3, and $b = 2.0$.

5.4 Estimates of $\dot{N}_{\max}$ and $m_{\text{event,min}}$

$\dot{N}_{\max}$ and $m_{\text{event,min}}$ were defined in Section 3.3. Equations (3.9) and (3.10) show how they can be estimated assuming the drop size distribution is known. Tables 5.1 and 5.2 present the measured drop size distribution and the calculation of $\dot{N}_{\max}$ for the spraying conditions used in Experiments E1 and E3 (see Table 4.2), respectively. The tables show the volume (mass) distribution of the spray as measured by the laser diffraction instrument. By using the average drop diameter $\bar{d}$, the mass of a single drop, m_{drop} is found for each size interval (row). Then the number of drops sprayed per unit time in each size interval is calculated in the last column. The sum is then the total number of drops sprayed per unit time which is $\dot{N}_{\max}$.

In case of the spray used in Experiment E1, Table 5.1 shows that $\dot{N}_{\max} = 3.01 \cdot 10^8 \text{s}^{-1}$. Equation (3.10) gives the following result:

$$m_{\text{event,min}} = \frac{\dot{m}_{\text{spray}}}{\dot{N}_{\max}} = \frac{6.33 \cdot 10^{-5} \text{kgs}^{-1}}{3.01 \cdot 10^8 \text{s}^{-1}} = 2.10 \cdot 10^{-13} \text{kg} \tag{5.6}$$

Similarly, in case of the spray used in Experiment E3, Table 5.2 shows that $\dot{N}_{\max} = 1.61 \cdot 10^9 \text{s}^{-1}$, and $m_{\text{event,min}}$ becomes

$$m_{\text{event,min}} = \frac{\dot{m}_{\text{spray}}}{\dot{N}_{\max}} = \frac{3.4 \cdot 10^{-4} \text{kgs}^{-1}}{1.61 \cdot 10^9 \text{s}^{-1}} = 2.11 \cdot 10^{-13} \text{kg} \tag{5.7}$$

In both tables it can be observed that the major contribution to $\dot{N}_{\max}$ comes from the smaller size intervals, and it can be seen that for these intervals the volume distribution is very similar. This explains why the two above results for $m_{\text{event,min}}$ are almost identical. It is also emphasized that the calculated values are estimates showing the order of magnitude and not exact values. One reason for this is that slight uncertainties in the smaller size intervals of the drop size distribution have great influence on $\dot{N}_{\max}$. For example, the laser diffraction instrument might show the volume fraction of the smallest size interval as 0.1 %, even if the "true" value was 0.1499 %. This means that the real number of drops per unit time in that size interval would be almost 50 % higher than the one estimated. In Section 5.5, it is shown that actual values of $m_{\text{event}} \gg m_{\text{event,min}}$. This could indicate that the major number of small drops dry out quickly so that they never get involved in potential agglomeration events. It is possible that the definition of $\dot{N}_{\max}$ should be changed so that only drop sizes over a critical minimum size should be considered. Further work is needed to determine this.

	[g/min]	[kg/s]
$\dot{m}_{\text{spray}}$	3.8	6.33E-05

$d_{\min}$	$d_{\max}$	$\overline{d}$	f_v	m_{drop}	$\dot{N}$
[1e-6 m]	[1e-6 m]	[1e-6 m]	[%]	[kg]	[#]
0	1.5	0.8	0.1	2.2E-16	2.9E+08
1.5	5.8	3.7	0.3	2.5E-14	7.5E+06
5.8	6.7	6.3	0.2	1.3E-13	9.9E+05
6.7	7.8	7.3	0.3	2.0E-13	9.5E+05
7.8	9.1	8.4	0.3	3.1E-13	6.1E+05
9.1	10.4	9.7	0.5	4.8E-13	6.6E+05
10.4	12.1	11.3	0.8	7.5E-13	6.8E+05
12.1	14.1	13.1	1.1	1.2E-12	5.9E+05
14.1	16.3	15.2	1.2	1.8E-12	4.1E+05
16.3	18.9	17.6	1.5	2.9E-12	3.3E+05
18.9	21.9	20.4	2.1	4.4E-12	3.0E+05
21.9	25.4	23.7	2.9	6.9E-12	2.7E+05
25.4	29.5	27.5	3.8	1.1E-11	2.2E+05
29.5	34.1	31.8	4.4	1.7E-11	1.7E+05
34.1	39.5	36.8	5.5	2.6E-11	1.3E+05
39.5	45.8	42.7	6.9	4.1E-11	1.1E+05
45.8	53.0	49.4	7.4	6.3E-11	7.4E+04
53.0	61.5	57.3	7.4	9.8E-11	4.8E+04
61.5	71.5	66.5	6.1	1.5E-10	2.5E+04
71.5	82.5	77.0	5.1	2.4E-10	1.4E+04
82.5	96.0	89.3	6.0	3.7E-10	1.0E+04
96.0	111.0	103.5	6.1	5.8E-10	6.7E+03
111.0	129.0	120.0	5.8	9.0E-10	4.1E+03
129.0	150.0	139.5	5.0	1.4E-09	2.2E+03
150.0	173.0	161.5	4.3	2.2E-09	1.2E+03
173.0	201.0	187.0	3.7	3.4E-09	6.8E+02
201.0	233.0	217.0	3.1	5.4E-09	3.7E+02
233.0	270.0	251.5	2.4	8.3E-09	1.8E+02
270.0	313.0	291.5	1.8	1.3E-08	8.8E+01
313.0	362.0	337.5	1.4	2.0E-08	4.4E+01
362.0	420.0	391.0	1.0	3.1E-08	2.0E+01
420.0	487.0	453.5	0.8	4.9E-08	1.0E+01
487.0	564.0	525.5	0.7	7.6E-08	5.8E+00
			100.0		3.01E+08

Table 5.1: Calculation of $\dot{N}_{\max}$. Low spray rate.

	[g/min]	[kg/s]
$\dot{m}_{spray}$	20.5	3.4E-04

d_{min}	d_{max}	$\overline{d}$	f_v	m_{drop}	$\dot{N}$
[1e-6 m]	[1e-6 m]	[1e-6 m]	[%]	[kg]	[#]
0.0	1.5	0.8	0.1	2.2E-16	1.5E+09
1.5	5.8	3.7	0.3	2.5E-14	4.0E+07
5.8	6.7	6.3	0.2	1.3E-13	5.3E+06
6.7	7.8	7.3	0.2	2.0E-13	3.4E+06
7.8	9.1	8.4	0.2	3.1E-13	2.2E+06
9.1	10.4	9.7	0.3	4.8E-13	2.1E+06
10.4	12.1	11.3	0.5	7.5E-13	2.3E+06
12.1	14.1	13.1	0.6	1.2E-12	1.7E+06
14.1	16.3	15.2	0.6	1.8E-12	1.1E+06
16.3	18.9	17.6	0.9	2.9E-12	1.1E+06
18.9	21.9	20.4	1.4	4.4E-12	1.1E+06
21.9	25.4	23.7	1.7	6.9E-12	8.4E+05
25.4	29.5	27.5	1.8	1.1E-11	5.7E+05
29.5	34.1	31.8	2.2	1.7E-11	4.5E+05
34.1	39.5	36.8	3.2	2.6E-11	4.2E+05
39.5	45.8	42.7	4.6	4.1E-11	3.9E+05
45.8	53.0	49.4	4.2	6.3E-11	2.3E+05
53.0	61.5	57.3	3.5	9.8E-11	1.2E+05
61.5	71.5	66.5	4.2	1.5E-10	9.3E+04
71.5	82.5	77.0	5.3	2.4E-10	7.6E+04
82.5	96.0	89.3	7.1	3.7E-10	6.5E+04
96.0	111.0	103.5	7.1	5.8E-10	4.2E+04
111.0	129.0	120.0	6.5	9.0E-10	2.5E+04
129.0	150.0	139.5	5.7	1.4E-09	1.4E+04
150.0	173.0	161.5	5.7	2.2E-09	8.8E+03
173.0	201.0	187.0	6.0	3.4E-09	6.0E+03
201.0	233.0	217.0	5.8	5.4E-09	3.7E+03
233.0	270.0	251.5	5.1	8.3E-09	2.1E+03
270.0	313.0	291.5	4.2	1.3E-08	1.1E+03
313.0	362.0	337.5	3.4	2.0E-08	5.8E+02
362.0	420.0	391.0	2.8	3.1E-08	3.1E+02
420.0	487.0	453.5	2.4	4.9E-08	1.7E+02
487.0	564.0	525.5	2.2	7.6E-08	9.9E+01
			100.0		1.61E+09

Table 5.2: Calculation of $\dot{N}_{max}$. High spray rate.

5.5 The Effect of the Spray Rate

Three experiments (termed E1, E2, and E3 in Table 4.2) were simulated to see the effect of the spray rate on the first model parameter, m_{event}. It was assumed that all potential agglomeration events were successful (all $\alpha_{j,k} = 1$). The assumption seems reasonable because the simulated experiments do not show any sign of entering the layering growth regime (the mass mean diameter in Figure 4.4 does not level off). This implies that the model parameters b and m^* are no longer of interest, only m_{event} has to be fitted to experimental data, which keeps things simple when finding a value for the model parameter. The simple criterion of the simulated mass median diameter being equal to the experimental mass median diameter was used to determine the value of m_{event}.

Because the spray rate was varied in the experiments, liquid sprayed is a better measure of the extent of the process than time. The first sampled PSDs were taken at 150 g liquid sprayed, in case of the Experiments E2 and E3. Therefore, this was chosen as the final point of the simulations. In Figures 5.7 to 5.9, the simulation results of the three experiments (using a low, medium, and high spray rate) can be seen. It can be observed that the upper part of the predicted PSD lies somewhat to the right of the experimental PSD. The reason may be that the assumption of all $\alpha_{j,k} = 1$ is too crude, or that the submodel for $p_{j,k}$ could be improved. However, a perfect fit is not to be expected because of the many challenges of comparing predicted and experimental PSDs as discussed in Section 5.2.

The fitting of the model parameter, m_{event} to the experimental data resulted in Figure 5.10 which shows m_{event} as a decreasing function of spray rate. This can be explained by using Figure 3.2. A higher spray rate will probably lead to more drop coalescence (decreasing $\dot{N}$) which means more liquid on the same particle and a longer drying time. This has the potential to reduce the effect of surface drying (increasing $\dot{N}$) and could very well explain the result. Another point is that a higher spray rate will increase the relative humidity of the outlet air which could result in less spray drying (increasing $\dot{N}$). If the assumption that $\alpha_{j,k} = 1$ is too crude, the values in Figure 5.10 represent an overprediction of m_{event}. This is because of the actual larger number of potential agglomeration events (larger $\dot{N}$) then acting in combination with a lower fraction of successful agglomeration events.

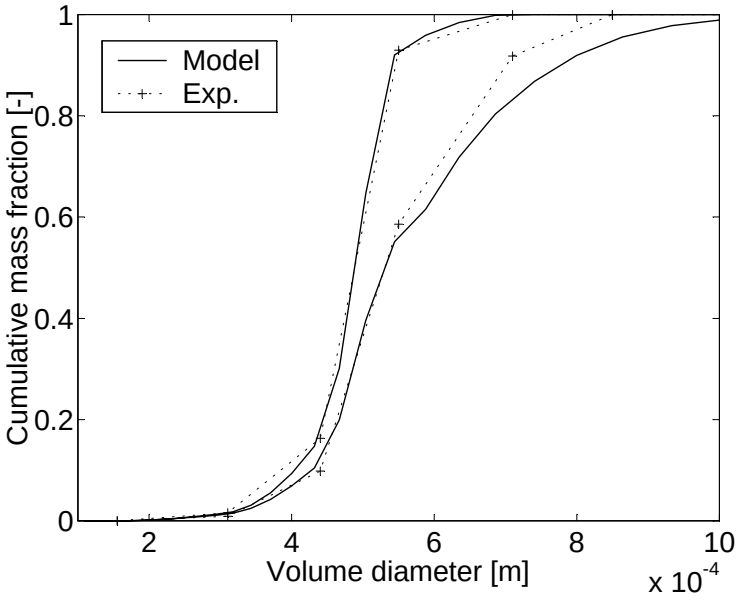

Figure 5.7: Simulation of Experiment E1 in Table 4.2 (low spray rate). The simulation time was from $t = 0$ to $t = 2400$ s (152 g liquid sprayed).

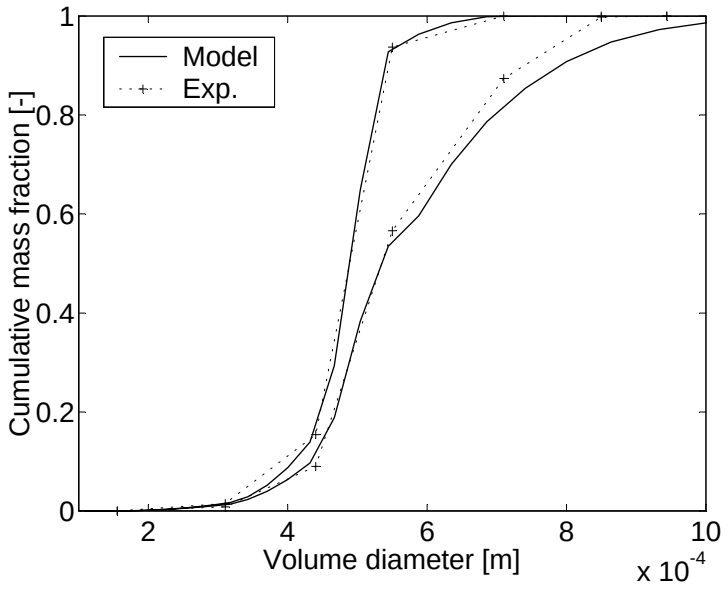

Figure 5.8: Simulation of Experiment E2 in Table 4.2 (medium spray rate). The simulation time was from $t = 0$ to $t = 698$ s (150 g liquid sprayed).

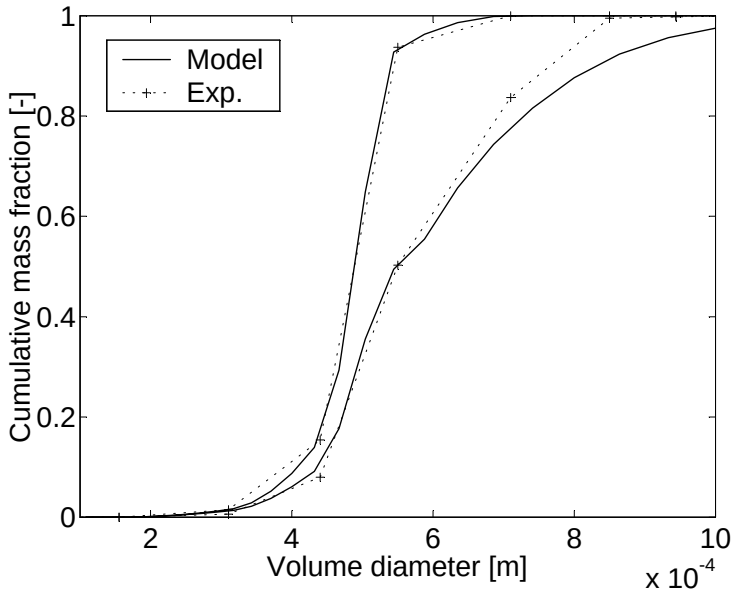

Figure 5.9: Simulation of Experiment E3 in Table 4.2 (high spray rate). The simulation time was from $t = 0$ to $t = 440$ s (150 g liquid sprayed).

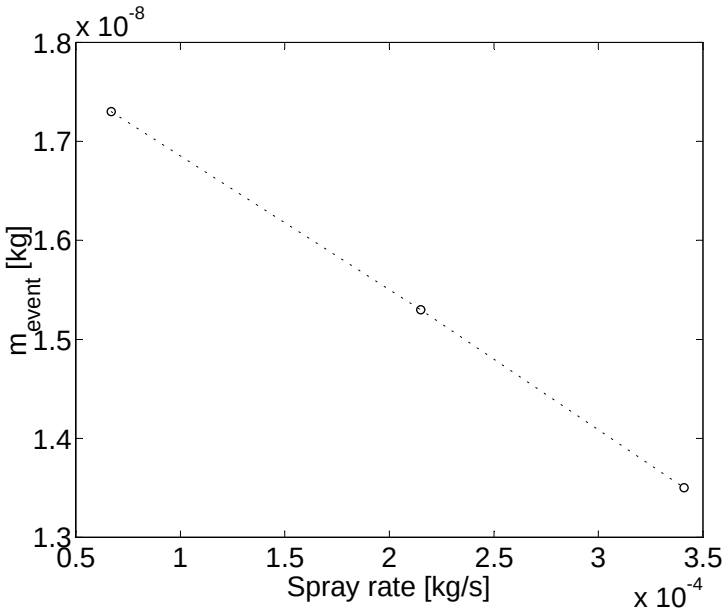

Figure 5.10: Graph showing the effect of spray rate ($\dot{m}_{\text{spray}}$) on the model parameter, m_{event}.

5.6 The Effect of the Bed Temperature

Three experiments (termed E1, E5, and E6 in Table 4.2) were simulated to see the effect of the bed temperature on the first model parameter, m_{event}. Once again, it was assumed that all potential agglomeration events were successful (all $\alpha_{j,k} = 1$), and the criterion of the simulated mass median diameter being equal to the experimental mass median diameter was used to determine the value of m_{event}. Since the spray rate was constant in these experiments, time was used as a measure of the extent of the process. The sampled PSDs taken after 40 minutes of granulation were chosen as the final point of the simulations. The simulation results of the three experiments (using a high, medium, and a low bed temperature) are presented in Figures 5.11 to 5.13.

The fitting of the model parameter, m_{event} to the experimental data gave the result seen in Figure 5.14 which shows m_{event} as an increasing tendency of bed temperature. This can be explained by looking at Figure 3.2. A higher bed temperature will lead to a shorter drying time/ faster drying (see the next section). This increases the effect of surface drying (decreasing $\dot{N}$) and explains why more liquid must be sprayed per potential agglomeration event (higher m_{event}). A higher bed temperature will also increase the effect of spray drying (decreasing $\dot{N}$).

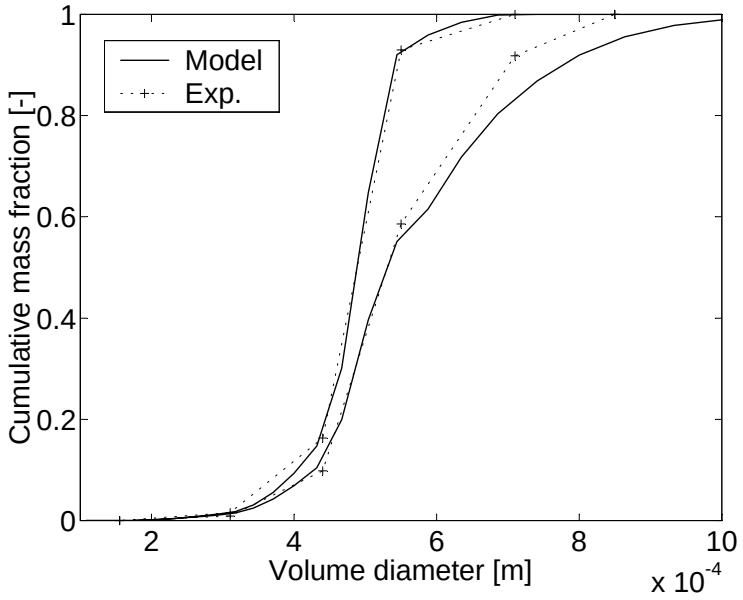

Figure 5.11: Simulation of Experiment E1 in Table 4.2 ($T_{\text{bed}} = 85$ °C). The simulation time was from $t = 0$ to $t = 2400$ s.

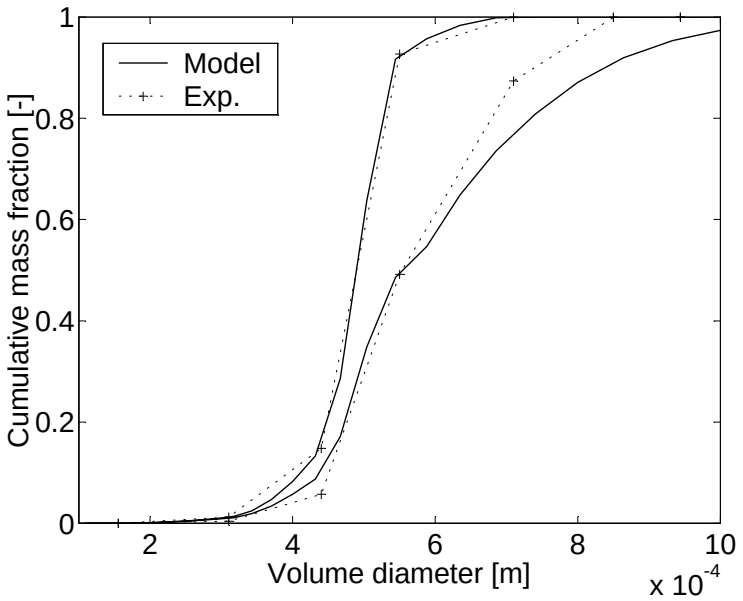

Figure 5.12: Simulation of Experiment E5 in Table 4.2 ($T_{\text{bed}} = 70$ °C). The simulation time was from $t = 0$ to $t = 2400$ s.

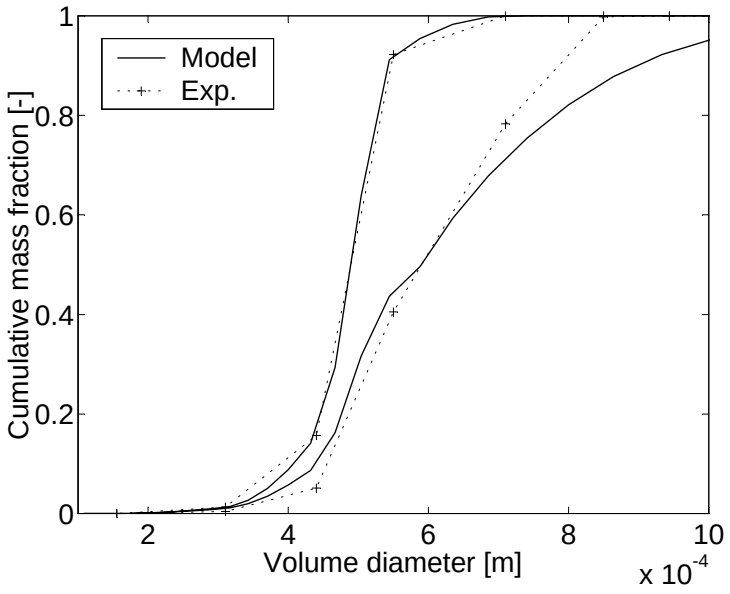

Figure 5.13: Simulation of Experiment E6 in Table 4.2 ($T_{\text{bed}} = 55$ °C). The simulation time was from $t = 0$ to $t = 2400$ s.

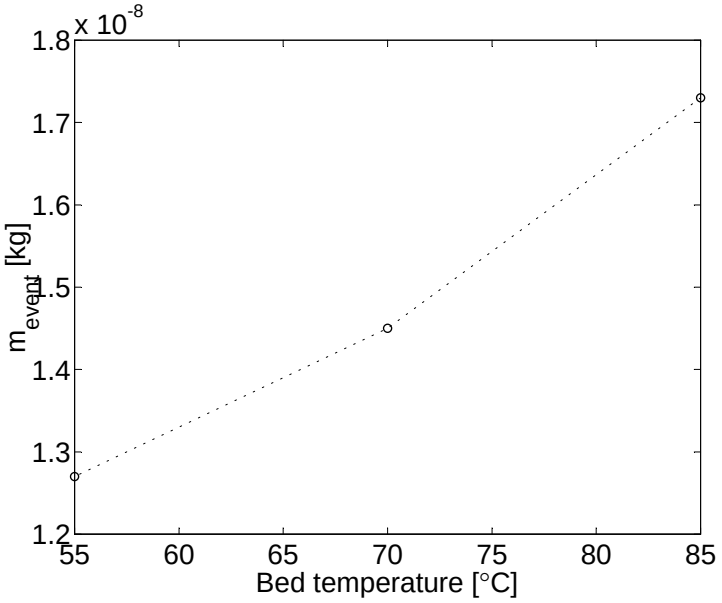

Figure 5.14: Graph showing the effect of bed temperature on the model parameter, m_{event}.

5.6.1 Estimates of a Particle's Drying Time

In order to understand the effect of bed temperature on the drying rate, a simplified situation was analysed. Figure 5.15 shows a spherical particle, which is covered by a liquid water layer, placed in a drying air flow. The air has velocity U, temperature T_{air}, and the density of its water vapor is $\rho_{\mathrm{H_2O}}$. Just above the water surface, the density of the water vapor is $\rho^*_{\mathrm{H_2O}}$ which is a function of the temperature of the liquid layer, T_l. Because of the density difference $\rho^*_{\mathrm{H_2O}}(T_l) - \rho_{\mathrm{H_2O}}$, water in the liquid layer evaporates. This evaporation rate is

$$\dot{m}_{\mathrm{H_2O}} = Ak_{\mathrm{g}}(\rho^*_{\mathrm{H_2O}}(T_{\mathrm{l}}) - \rho_{\mathrm{H_2O}}) \tag{5.8}$$

where A is the surface area and k_{g} is the mass transfer coefficient. Because of the temperature difference of the air and the liquid layer, the rate of heat transfer from the air flow to the liquid layer is

$$\dot{Q}_{\mathrm{conv}} = Ah(T_{\mathrm{air}} - T_{\mathrm{l}}) \tag{5.9}$$

If the resistance against heat transfer between the liquid layer and the centre of the particle is small, heat conduction is very fast so that the particle temperature, T_p equals T_l. This is a good assumption if the Biot number is smaller than 0.1. A later estimate (see Equation (5.12)) shows that this is the case. The heat balance equation for the particle becomes

$$(c_{\mathrm{p}}m_{\mathrm{p}} + c_{\mathrm{l}}m_{\mathrm{l}})\frac{\mathrm{d}T_{\mathrm{p}}}{\mathrm{d}t} = \dot{Q}_{\mathrm{conv}} - \dot{m}_{\mathrm{H_2O}}\Delta h \tag{5.10}$$

where c_{p} and c_{l} are the heat capacities of the particle and the liquid, respectively. Δh is the heat of evaporation at T_l. The mass balance equation for the liquid layer is

$$\frac{\mathrm{d}m_{\mathrm{l}}}{\mathrm{d}t} = -\dot{m}_{\mathrm{H_2O}} \tag{5.11}$$

A computer program *evap_sim* was written in Fortran 90 to solve the above equations. It is assumed that a drop of specified size spreads out over the spherical particle to form a liquid layer of uniform thickness. Initially, this layer has a specified temperature that may differ from that of the particle. However, after the first time step, a common temperature for the particle and the liquid is calculated because of the low internal resistance to heat transfer. The heat and mass transfer coefficients are found using Equations (2.2) and (2.3). When $m_{\mathrm{l}} = 0$, the calculation is stopped, and the time used is the drying time. The program can also simulate heat conduction inside the particle by dividing the sphere into a number of shells. Each shell then has its own heat balance equation. It was found, however, that the discretization had little effect on the drying time obtained. This result

can be explained by the low Biot number which is estimated to be (in case of a 400 μm diameter sphere of sodium chloride)

$$\mathrm{Bi} = \frac{h\frac{R}{3}}{k} = \frac{(180.0)\cdot(\frac{400\cdot 10^{-6}/2}{3})}{5.4} = 2.2\cdot 10^{-3} \ll 0.1 \tag{5.12}$$

Figure 5.16 shows the estimated drying time as a function of air temperature for a spherical sodium chloride particle with diameter 400 μm covered by a liquid layer originating from a drop with diameter 100 μm. An increase in the drop diameter to 200 μm, results in significantly longer drying times (see Figure 5.17). In both cases, it is observed as expected that the drying time is a decreasing function of air temperature.

The result in Figure 5.14 can be explained qualitatively by the graphs in figs. 5.16 and 5.17 which show the drying time as a decreasing function of temperature. A higher bed temperature will therefore cause shorter drying times and fewer collisions where surface liquid is present. This means that the number of potential agglomeration events per unit time is reduced, as observed in Figure 5.14.

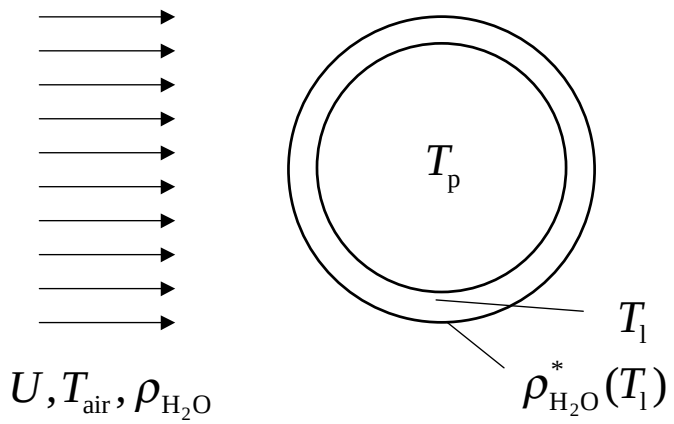

Figure 5.15: An air flow passes over a solid sphere covered by a liquid water layer causing evaporation.

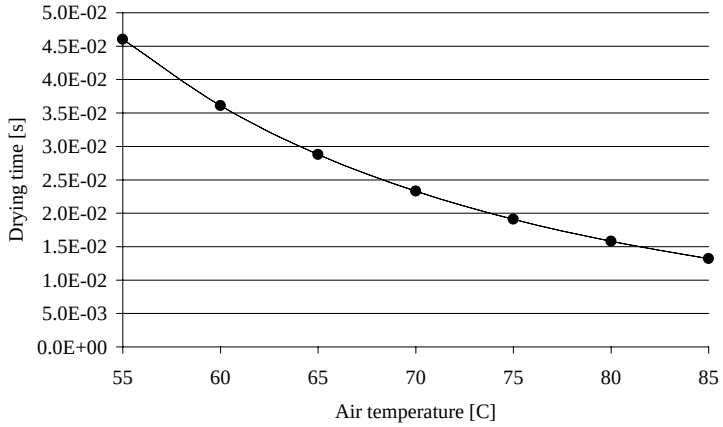

Figure 5.16: A particle's drying time as function of air temperature. A drop with diameter 100 μm has initially formed a film around the spherical particle with diameter 400 μm.

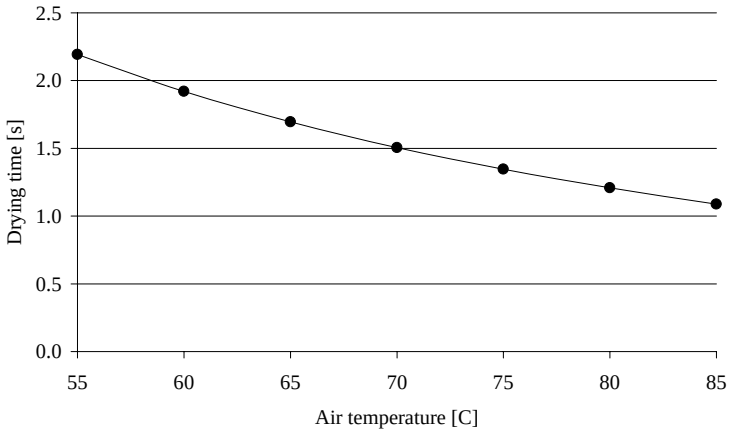

Figure 5.17: A particle's drying time as function of air temperature. A drop with diameter 200 μm has initially formed a film around the spherical particle with diameter 400 μm.

5.7 Simulation of Experiment E2

In a longer experiment where a critical PSD is reached and further growth only takes place by the layering mechanism, one can no longer assume that all agglomeration events are successful. Experiment E2 in Table 4.2 is an example of such a situation. To describe this experiment successfully, it is neccessary to model $\alpha_{j,k}$. The following submodel was proposed in the last chapter:

$$\alpha_{j,k} = \begin{cases} 1 & \text{if} \quad M_{j,k} \leq M^* = 2^{(1-2b)} m^* \\ 0 & \text{if} \quad M_{j,k} > M^* = 2^{(1-2b)} m^* \end{cases} \tag{5.13}$$

where,

$$M_{j,k} = \frac{(m_j m_k)^b}{(m_j + m_k)^{2b-1}} \tag{5.14}$$

where m^* and b are the two model parameters which must be fitted to the experimental data.

Figure 5.18 shows a simulation of Experiment E2. The three model parameters stated in the figure caption were determined by trial and error. Qualitatively, the simulation agrees well with the experiment. An alternative method would be to use a numerical method to minimize an object function defined in some way to represent the deviation between the simulated and experimental PSDs. However, this strategy was not chosen in this work because the slighlty more "accurate" values of the model parameters were not needed. The purpose here was not to perform an extensive experimental study with the aim of proposing correlations between model parameters and operating conditions/ material properties. The main purpose of this chapter is to build a qualitative understanding of how the model parameters affects the evolving PSD.

Figure 3.9 on page 39 showed how the value of b affected the shape of the critical contour line representing the limit between successful and unsuccessful agglomeration. It is seen from the figure that a higher b-value means that the area of successful agglomeration events increases, while a lower b-value means that the same area decreases. Simply put, a high b-value indicates that both small-small and small-large particle interactions are successful while large-large particle interactions are not. On the other hand, a low b-value indicates that only small-small interactions are successful.

Figure 5.19 shows how a too high b-value affects the simulation. Because the area of successful agglomeration is too large, the simulated PSD does not approach the final PSD but the agglomeration process continues too far. Figure 5.20 shows how a too low b-value affects the simulation. Now,

the area of successful agglomeration becomes too small, so the simulated PSD reaches a critical PSD before it should and the final PSD is never obtained. It can also be seen that the simulated PSD is more narrow because small-small intercations are favored by lower b-values.

In Section 3.5, m^* was defined as the particle mass of the largest two equally sized particles that can successfully agglomerate. Figure 5.21 shows the effect of a too high m^*-value on the simulation. The critical PSD is shifted to the right. Figure 5.22 shows the effect of a too low m^*-value. The critical PSD is then shifted to the left.

The above examples show that the model parameters b and m^* determine the shape and position of the critical PSD and if a critical PSD is reached at all. Figure 5.23 shows the effect of a too high m_{event}-value on the simulation. The critical PSD is the the same, but it can be seen that the PSD evolves too slowly.

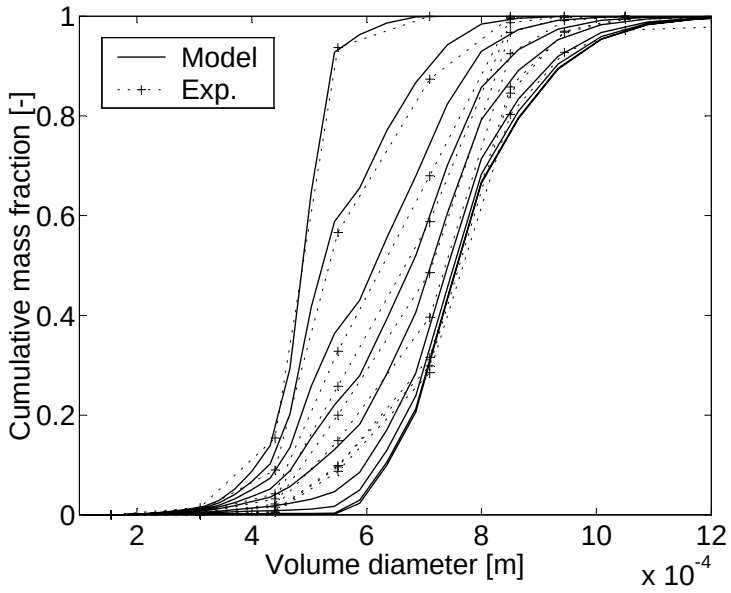

Figure 5.18: Simulation of Experiment E2 in Table 4.2. The model parameters used are $m_{\text{event}} = 1.8 \cdot 10^{-8}$ kg, $m^* = 2.15 \cdot 10^{-7}$ kg, and $b = 1.5$.

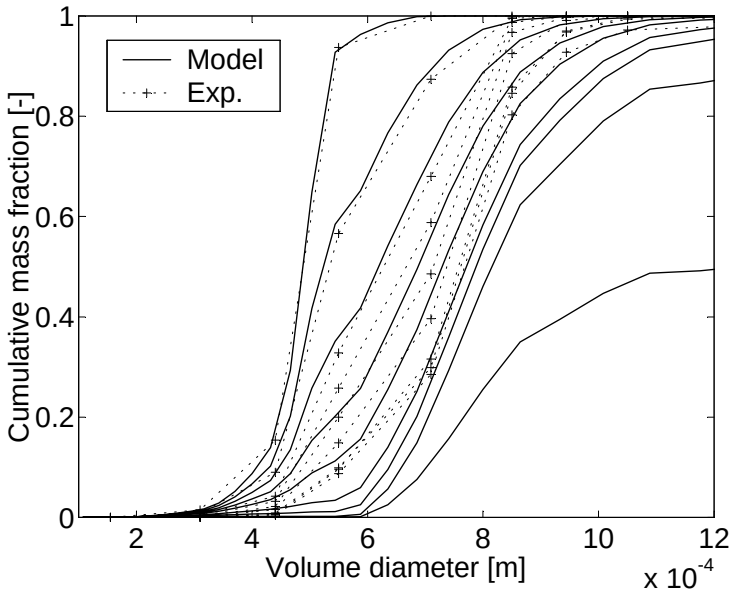

Figure 5.19: Simulation of Experiment E2 in Table 4.2. The model parameters used are $m_{\text{event}} = 1.8 \cdot 10^{-8}$ kg, $m^* = 2.15 \cdot 10^{-7}$ kg, and $b = 2.0$.

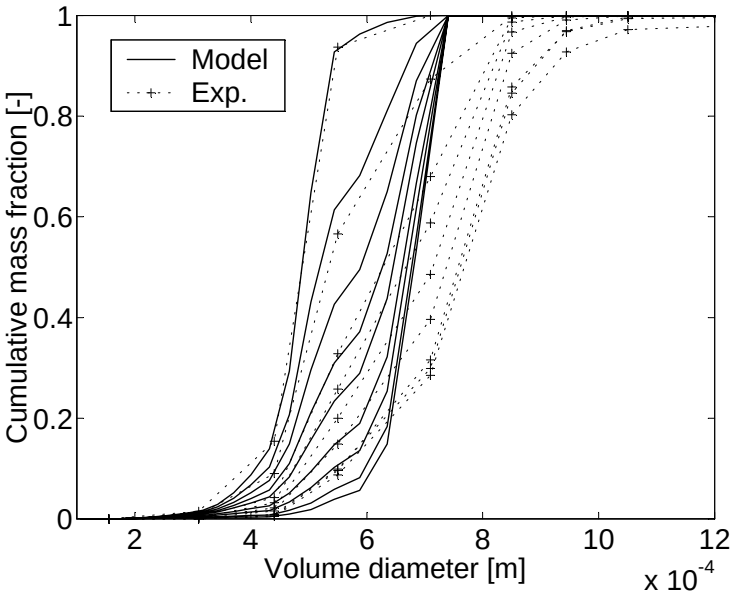

Figure 5.20: Simulation of Experiment E2 in Table 4.2. The model parameters used are $m_{\text{event}} = 1.8 \cdot 10^{-8}$ kg, $m^* = 2.15 \cdot 10^{-7}$ kg, and $b = 0.0$.

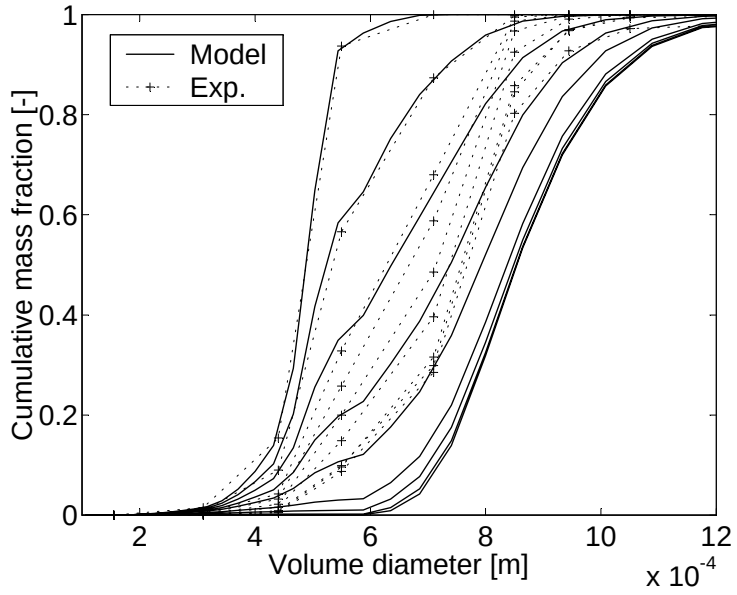

Figure 5.21: Simulation of Experiment E2 in Table 4.2. The model parameters used are $m_{\text{event}} = 1.8 \cdot 10^{-8}$ kg, $m^* = 3.0 \cdot 10^{-7}$ kg, and $b = 1.5$.

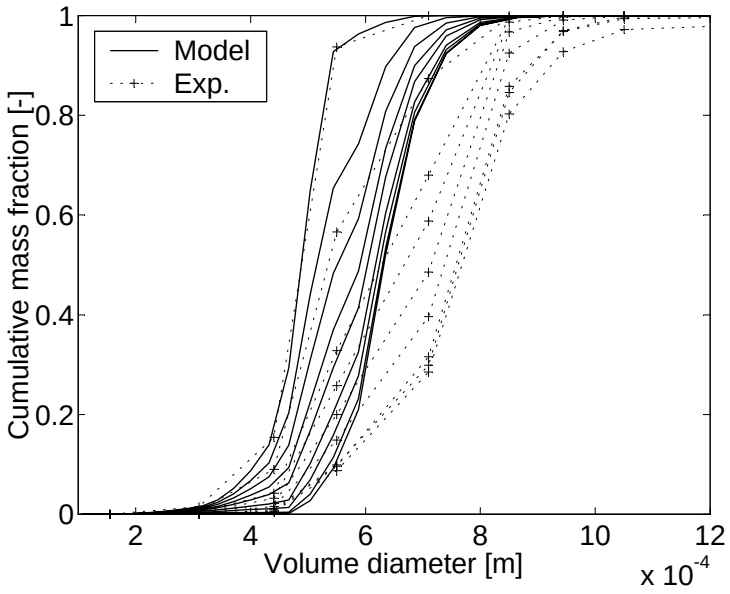

Figure 5.22: Simulation of Experiment E2 in Table 4.2. The model parameters used are $m_{\text{event}} = 1.8 \cdot 10^{-8}$ kg, $m^* = 1.5 \cdot 10^{-7}$ kg, and $b = 1.5$.

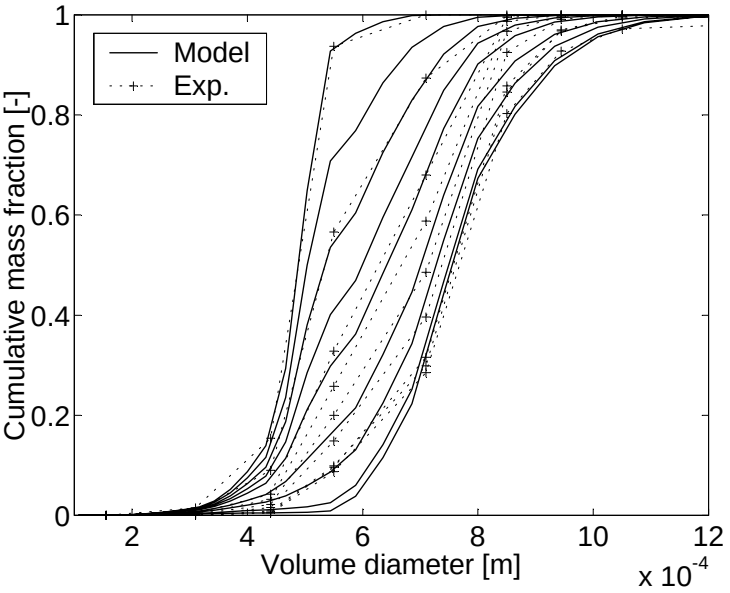

Figure 5.23: Simulation of Experiment E2 in Table 4.2. The model parameters used are $m_{\text{event}} = 3.0 \cdot 10^{-8}$ kg, $m^* = 2.15 \cdot 10^{-7}$ kg, and $b = 1.5$.

Chapter 6

Conclusions and Recommendations

6.1 Conclusions

Agglomeration is often the dominant growth mechanism in granulation processes where the goal is to enlarge the size of solid particles. If only two particles stick together in an agglomeration event, this is referred to here as binary agglomeration. Population balance modeling is today the obvious tool for the simulation of the evolution of the particle size distribution (PSD) in a binary agglomeration process. The essential challenge is the modeling of the kinetic terms for binary agglomeration in the population balance equation (PBE). These kinetic terms give the birth and death rates of particles as a function of particle size. The PBE with its kinetic terms is referred to here as a population balance model framework for binary agglomeration.

A new population balance model framework for binary agglomeration has been proposed (see Section 3.2). It consists of the three submodels $\dot{N}$, $p_{j,k}$, and $\alpha_{j,k}$ defined respectively as the number of potential agglomeration events per unit time, the probability of a potential agglomeration event involving particles from size intervals j and k, and the probability of successful agglomeration. The product $\dot{N}p_{j,k}\alpha_{j,k}$ represents the birth rate of agglomerates due to agglomeration between particles in size intervals j and k (see Equation (3.5)). Assuming expressions for the three submodels can be found, this new model framework can be applied to any binary agglomeration process. This generality represents an improvement over previous coalescence kernel formulations (see Equation (2.17) and Section 2.9.3) which implicate that the particle collision frequency is rate limiting for the agglomeration kinetics. It was shown in Section 3.7, that the coalescence kernel model of Adetayo and Ennis [1], which is considered to

be the state-of-the-art model, represents a special case of the new model framework. The numerical method of Kumar and Ramkrishna [35], which was used to solve the PBE, was modified so that it could be applied to the new model framework. This was necessary because their method assumed the use of a coalescence kernel model. The modification resulted in a new set of ordinary differential equations given in Section 3.8.

A new specific model for fluidized bed granulation (FBG) was proposed by choosing expressions for the three submodels $\dot{N}$, $p_{j,k}$, and $\alpha_{j,k}$ (see Sections 3.3 to 3.5). All model equations are summarized on p. 41. The two first submodels $\dot{N}$ and $p_{j,k}$ were proposed and the third submodel $\alpha_{j,k}$ was taken from Adetayo and Ennis [1], but formulated differently by using the model parameter m^* with a clearer physical interpretation than the original W^* (see Section 3.5). The three model parameters used are m_{event}, b, and m^*. They are respectively the liquid mass sprayed per potential agglomeration event, a parameter determining how easily other particle combinations than small-small can successfully agglomerate, and the largest mass of a particle capable of successful agglomeration with another particle of equal size. The new model underscores the fact that the presence of liquid, and not the collision frequency, is rate limiting in FBG. An advantage of the new FBG model is that a maximum number of agglomeration events per unit time can be estimated (see Section 3.3). This means that the model is one step closer to being used predictively.

Experiments in a batch fluidized bed granulator were carried out (see Chapter 4). The results of these could be described by the new model. The effect of spray rate and bed temperature on the first model parameter, m_{event} was qualitatively explained by physical mechanisms like drop coalescence, surface drying, and spray drying. It was found that m_{event} was a decreasing function of spray rate and an increasing function of bed temperature (see Figures 5.10 and 5.14). A long experiment (E2 in Table 4.2) in which a critical PSD was reached (agglomeration stopped) was well described by choosing proper values for the second and third model parameter, b and m^* in the submodel for $\alpha_{j,k}$ (see Figure 5.18).

6.2 Recommendations for Further Work

Today, no a priori population balance models exist to predict agglomerate growth in granulation processes like FBG. All models have parameters that must be fitted to experimental data. This is also the case with the new model framework applied to FBG where the three model parameters m_{event}, b, and m^* are unknown functions of operating conditions and material properties. A great challenge for further work is therefore to develop

predictive submodels with model parameters related to physics. In the ideal situation one would have the model parameters explicitly expressed as functions of dimensionless groups including material properties and operating conditions. To identify such groups that capture the most essential agglomeration physics, would therefore be of great value.

In the a priori prediction of $\dot{N}$, the discrete element method (DEM) may be the way to go. "Numerical experiments" using DEM could prove to be an interesting alternative, because it may be difficult to determine $\dot{N}$ experimentally. DEM has the potential to simulate spray drying, drop coalescence on particle surfaces, and drying of the wetted surfaces. The motion of all single particles is also simulated. With DEM it is, in principle, possible to calculate the number of collisions per unit time where liquid is present. This number would then be an estimate of $\dot{N}$. A correlation for $\dot{N}$ could then possibly be acheived by altering variables like superficial gas velocity, spray rate, drop size and particle size distribution.

$p_{j,k}$ has the potential to include effects like segregation. Instead of the fluidized bed being perfectly mixed, a higher relative concentration of fine particles may be present in the upper zone of the bed where agglomeration takes place. This could be included in a future submodel. Further work is also needed to determine if the proposed form of $p_{j,k}$ expressed as a function of area fractions is the best choice (see Section 3.4).

Relating the model parameters b and m^* in the submodel for $\alpha_{j,k}$ to material properties and operating conditions is another difficulty. The balance between attractive and separating forces will determine if a potential agglomeration event is successful or not. Effects that increase the attractive force of a liquid bridge will increase m^*, while effects that cause more agitation and intense collisions will decrease m^*. More experiments on the particle level like the one of Simons and Fairbrother [77] where attractive forces of liquid bridges are measured need to carried out to be able to make predictions. It is also necessary to understand the separating forces better. A possible experiment might be to introduce particle couples connected with solid bridges into a fluidized bed at certain conditions. The material properties and geometry of these solid bridges would be known and could be varied in different experiments. After an experiment the particle couple may or may not be broken. By varying variables like fluidization velocity and particle size, one would gain an understanding of the effect on the separating forces. The understanding of attractive and separating forces need to be combined to predict if a potential agglomeration event is successful or not.

Bibliography

[1] A. A. Adetayo and B. J. Ennis. Unifying approach to modeling granule coalescence mechanisms. *AIChE Journal*, 43(4):927–934, 1997.

[2] A. A. Adetayo and B. J. Ennis. A new approach to modeling granulation processes for simulation and control purposes. *Powder Technology*, 108:202–209, 2000.

[3] A. A. Adetayo, J. D. Litster, S. E. Pratsinis, and B. J. Ennis. Population balance modelling of drum granulation of materials with wide size distribution. *Powder Technology*, 82:37–49, 1995.

[4] J. Baeyens and D. Geldart. *Gas Fluidization Technology*, chapter Solids mixing. John Wiley & Sons, 1986.

[5] R.-D. Becher. *Untersuchung der Agglomeration von Partikeln bei der Wirbelschicht-Sprügranulation.* Dissertation, Universität Fridericiana Karlsruhe (Technische Hochschule), 1997.

[6] R.-D. Becher and E.-U. Schlünder. Fluidized bed granulation - the importance of a drying zone for the particle growth mechanism. *Chemical Engineering and Processing*, 37:1–6, 1998.

[7] R. B. Bird, W. E. Stewart, and E. N. Lightfoot. *Transport Phenomena.* John Wiley & Sons, 1960.

[8] A. Boemer, H. Qi, and U. Renz. Verification of eulerian simulation of spontaneous bubble formation in a fluidized bed. *Chemical Engineering Science*, 53:1835–1846, 1998.

[9] R. S. Brodkey, D. S. Kim, and W. Sidner. Fluid to particle heat transfer in a fluidized bed and to single particles. *Int. J. Heat Mass Transfer*, 34(9):2327–2337, 1990.

[10] R. Clift and J. R. Grace. *Fluidization*, chapter Continuous Bubbling and Slugging. Academic Press, 1985.

[11] J. P. Couderc. *Fluidization*, chapter Incipient Fluidization and Particulate Systems. Academic Press, 1985.

[12] S. A. Cryer. Modeling agglomeration processes in fluid-bed granulation. *AIChE Journal*, 45(10):2069–2078, 1999.

[13] J. F. Davidson, R. Clift, and D. Harrison, editors. *Fluidization*. Academic Press, 1985.

[14] B. J. Ennis. A micro-level based characterization of granulation phenomena. *Powder Technology*, 65:257–272, 1991.

[15] B. J. Ennis. Agglomeration and size enlargement. Session summary paper. *Powder Technology*, 88:203–225, 1996.

[16] B. J. Ennis, J. Li, G. Tardos, and R. Pfeffer. The influence of viscosity on the strength of an axially strained pendular liquid bridge. *Chemical Engineering Science*, 45(10):3071–3088, 1990.

[17] D. Geldart. Types of gas fluidization. *Powder Technology*, 7:285–292, 1972.

[18] D. Geldart, editor. *Gas Fluidization Technology*. John Wiley & Sons, 1986.

[19] Yinghe He. A criterion for particle agglomeration by collision. *Powder Technology*, 103:189–193, 1999.

[20] S. Heinrich. *Modellierung des Wärme- und Stoffübergangs sowie der Partikelpopulationen bei der Wirbelschicht-Sprühgranulation*. Dissertation, Universität Magdeburg, 2001.

[21] S. Heinrich and L. Morl. Fluidized bed spray granulation - A new model for the description of particle wetting and of temperature and concentration distribution. *Powder Technology*, 38:635–663, 1999.

[22] M. J. Hounslow. A discretized population balance for continous systems at steady state. *AIChE Journal*, 36(1):106–116, 1990.

[23] M. J. Hounslow, R. L. Ryall, and V. R. Marshall. A discretised population balance for nucleation, growth and aggregation. *AIChE Journal*, 34(11):1821–1832, 1988.

[24] S. M. Iveson. Granule coalescence modelling: Including the effects of bond strengthening and distributed impact separation forces. Submitted to Chemical Engineering Science, April 2000.

[25] S. M. Iveson. Limitations of one-dimensional population balance models of wet granulation. Submitted to Powder Technology, November 1999.

[26] S. M. Iveson and J. D. Litster. Growth regime map for liquid-bound granules. *AIChE Journal*, 44(7):1510–1518, 1998.

[27] S. M. Iveson and J. D. Litster. Liquid-bound granule impact deformation and coefficient of restitution. *Powder Technology*, 99:234–242, 1998.

[28] S. M. Iveson, J. D. Litster, and B. J. Ennis. Fundamental studies of granule consolidation. part 1: Effects of binder content and binder viscosity. *Powder Technology*, 88:15–20, 1996.

[29] S. M. Iveson, J. D. Litster, K. P. Hapgood, and B. J. Ennis. Nucleation, growth and breakage phenomena in agitated wet granulation processes: a review. *Powder Technology*, 117:3–39, 2001.

[30] O. Jonassen. *Heat Transfer to Immersed Horizontal Tubes in Gas Fluidized Bed Dryers.* Dissertation, Norwegian University of Technology and Science, 1999.

[31] P. C. Kapur. Kinetics of granulation by non-random coalescence mechanism. *Chemical Engineering Science*, 27:1863–1869, 1972.

[32] P. C. Kapur and D. W. Fuerstenau. A coalescence model for granulation. *I & C Process Design and Development*, 8(1):56–62, 1969.

[33] N. Kobayashi, R. Yamazaki, and S. Mori. A study on the behavior of bubbles in bubbling fluidized beds. *Powder Technology*, 113:327–344, 2000.

[34] J. A. M. Kuipers. Multilevel modelling of dispersed multiphase flows. *Oil & Gas Science and Technology — Rev. IFP*, 55:427–435, 2000.

[35] S. Kumar and D. Ramkrishna. On the solution of population balance equations by discretization - i. a fixed pivot technique. *Chemical Engineering Science*, 51(8):1311–1332, 1996.

[36] S. Kumar and D. Ramkrishna. On the solution of population balance equations by discretization - iii. nucleation, growth and aggregation of particles. *Chemical Engineering Science*, 52(24):4659–4679, 1997.

[37] D. Kunii and O. Levenspiel. *Fluidization Engineering.* Butterworth-Heinemann, second edition, 1991.

[38] G. Lian, C. Thornton, and M. J. Adams. Discrete particle simulation of agglomerate impact coalescence. *Chemical Engineering Science*, 53(19):3381–3391, 1998.

[39] K. C. Link. *Wirbelschicht-Sprügranulation. Untersuchung der Granulatbildung an einer frei schwebenden Einzelpartikel.* Dissertation, Universität Fridericiana Karlsruhe (Technische Hochschule), 1996.

[40] K. C. Link and E.-U. Schlünder. Fluidized bed spray granulation and film coating, a new method for the investigation of the coating process on a single sphere. *Drying Technology*, 15(6-8):1827–1843, 1997.

[41] J. D. Litster, K. P. Hapgood, J. N. Michaels, A. Sim, M. Roberts, S. K. Kameneni, and T. Hsu. Liquid distribution in wet granulation: dimensionless spray flux. *Powder Technology*, 114:29–32, 2001.

[42] J. D. Litster, D. J. Smit, and M. J. Hounslow. Adjustable discretized population balance for growth and aggregation. *AIChE Journal*, 41(3):591–603, 1995.

[43] L. X. Liu, J. D. Litster, S. M. Iveson, and B. J. Ennis. Coalescence of deformable granules in wet granulation processes. *AiChe Journal*, 46(3):529–539, 2000.

[44] S. Maronga. *On the Optimization of the Fluidized Bed Particulate Coating Process.* Dissertation, Royal Institute of Technology, Stockholm, 1998.

[45] S. J. Maronga and P. Wnukowski. The use of humidity and temperature profiles in optimizing the size of fluidized bed in a coating process. *Chemical Engineering and Processing*, 37:423–432, 1998.

[46] H. Martin. Heat and mass transfer in fluidized beds. *International Chemical Engineering*, 22(1):30–43, 1982.

[47] O. Maurstad, L. X. Liu, O. Bolland, and J. D. Litster. Experimental study of the particle size distribution in fluidized bed granulation. In *Proceedings of the 6th World Congress of Chemical Engineering*, Melbourne, Australia, 2001.

[48] A. F. Mills. *Heat and Mass Transfer.* Irwin, 1995.

[49] B. K. Mishra and C. Thornton. Impact breakage of particle agglomerates. *International Journal of Mineral Processing*, 61:225–239, 2001.

[50] A. W. Nienow. Fluidised bed granulation and coating: Applications to materials, agriculture and biotechnology. *Chem. Eng. Comm.*, 139:233–253, 1995.

[51] Z. Ormos. Studies on granulation in a fluidized bed i. methods for testing the physical properties of granulates. *Hungarian Journal of Industrial Chemistry*, 1:207–228, 1973.

[52] Z. Ormos, B. Csukas, and K. Pataki. Studies on granulation in a fluidized bed v. study on the particle size distribution of granulates. *Hungarian Journal of Industrial Chemistry*, 3:193–216, 1975.

[53] Z. Ormos, B. Csukas, and K. Pataki. Studies on granulation in a fluidized bed vi. granulation in mechanically agitated fluidized bed. *Hungarian Journal of Industrial Chemistry*, 3:631–646, 1975.

[54] Z. Ormos and K. Pataki. Studies on granulation in a fluidized bed vii. the effect of raw material upon granule formation. *Hungarian Journal of Industrial Chemistry*, 7:89–104, 1979.

[55] Z. Ormos and K. Pataki. Studies on granulation in a fluidized bed viii. effects of the raw material initial particle size upon granule formation. *Hungarian Journal of Industrial Chemistry*, 7:105–116, 1979.

[56] Z. Ormos, K. Pataki, and B. Csukas. Studies on granulation in a fluidized bed ii. the effects of the amount of the binder on the physical properties of granules formed in a fluidized bed. *Hungarian Journal of Industrial Chemistry*, 1:307–328, 1973.

[57] Z. Ormos, K. Pataki, and B. Csukas. Studies on granulation in a fluidized bed iii. calculation of the feed rate of granulating liquid. *Hungarian Journal of Industrial Chemistry*, 1:463–474, 1973.

[58] Z. Ormos, K. Pataki, and B. Csukas. Studies on granulation in a fluidized bed iv. effects of the characteristics of the fluidized bed the atomization and the air distributor upon the physical properties of the granulates. *Hungarian Journal of Industrial Chemistry*, 1:475–492, 1973.

[59] Z. Ormos, K. Pataki, and B. Stefko. Studies on granulation in a fluidized bed. x. effects of the relative amounts of various binders upon granule formation. *Hungarian Journal of Industrial Chemistry*, 7:141–152, 1979.

[60] Z. Ormos, K. Pataki, and B. Stefko. Studies on granulation in a fluidized bed.ix. effects of concentration of various binders upon granule formation. *Hungarian Journal of Industrial Chemistry*, 7:131–140, 1979.

[61] W. R. Paterson and A. N. Hayhurst. Shorter communication: Mass or heat transfer from a sphere to a flowing fluid. *Chemical Engineering Science*, 55:1925–1927, 2000.

[62] A. D. Randolph and M. A. Larson. *Theory of Particulate Processes.* Academic Press, second edition, 1988.

[63] W. E. Ranz and W. R. Marshall. Evaporation from drops. Part I. *Chemical Engineering Progress*, 48(3):141–146, 1952.

[64] W. E. Ranz and W. R. Marshall. Evaporation from drops. Part II. *Chemical Engineering Progress*, 48(4):173–180, 1952.

[65] S. H. Schaafsma, N. W. Kossen, M. T. Mos, L. Blauw, and A. C. Hoffmann. Effects and control of humidity and particle mixing in fluid-bed granulation. *AIChE Journal*, 45(6):1202–1210, 1999.

[66] S. H. Schaafsma, P. Vonk, and N. W. F. Kossen. Effects and control of humidity and particle mixing in fluid-bed granulation. *Int. Journal of Pharmaceutics*, 193:175–187, 2000.

[67] T. Schaefer and O. Worts. Control of fluidized bed granulation I. Effects of spray angle, nozzle height and starting materials on granule size and size distribution. *Arch. Pharm. Chemi. Sci.*, 5:51–60, 1977.

[68] T. Schaefer and O. Worts. Control of fluidized bed granulation II. Estimation of droplet size of atomized binder solutions. *Arch. Pharm. Chemi. Sci.*, 5:178–193, 1977.

[69] T. Schaefer and O. Worts. Control of fluidized bed granulation III. Effects of inlet air temperature and liquid flow rate on granule size and size distribution. Control of moisture content of granules in the drying phase. *Arch. Pharm. Chemi. Sci.*, 6:1–13, 1978.

[70] T. Schaefer and O. Worts. Control of fluidized bed granulation IV. Effects of binder solution and atomization on granule size and size distribution. *Arch. Pharm. Chemi. Sci.*, 6:14–25, 1978.

[71] T. Schaefer and O. Worts. Control of fluidized bed granulation V. Factors affecting granule growth. *Arch. Pharm. Chemi. Sci.*, 6:69–82, 1978.

[72] A. Schmidt and U. Renz. Eulerian computation of heat transfer in fluidized beds. *Chemical Engineering Science*, 54:5515–5552, 1999.

[73] J. P. K. Seville. The collective behaviour of particles. In *Proceedings of the 6th World Congress of Chemical Engineering*, Melbourne, Australia, 2001.

[74] J. P. K. Seville, C. D. Willett, and P. C. Knight. Interparticle forces in fluidisation: a review. *Powder Technology*, 113:261–268, 2000.

[75] P. A. Shamlou, Z. Liu, and J. G. Yates. Hydrodynamic influences on particle breakage in fluidized beds. *Chemical Engineering Science*, 45(4):809–817, 1990.

[76] P. J. Sherrington and R. Oliver. *Granulation*. Heyden & Son, 1981.

[77] S. J. R. Simons and R. J. Fairbrother. Direct observations of liquid binder-particle interactions: the role of wetting behaviour in agglomerate growth. *Powder Technology*, 110:44–58, 2000.

[78] S. J. R. Simons, J. P. K. Seville, and M. J. Adams. An analysis of the rupture energy of pendular liquid bridges. *Chemical Engineering Science*, 49(14):2331–2339, 1994.

[79] P. G. Smith and A. W. Nienow. Particle growth mechanisms in fluidised bed granulation - i. the effect of process variables. *Chemical Engineering Science*, 38(8):1223–1231, 1983.

[80] P. G. Smith and A. W. Nienow. Particle growth mechanisms in fluidised bed granulation - ii. comparison of experimental data with growth models. *Chemical Engineering Science*, 38(8):1233–1240, 1983.

[81] R. H. Snow, T. Allen, B. J. Ennis, and J. D. Litster. *Perry's Chemical Engineers' Handbook*, chapter Size Reduction and Size Enlargement. McGraw-Hill, second edition, 1997.

[82] M. Stein, Y. L. Ding, J. P. K. Seville, and D. J. Parker. Solids motion in bubbling gas fluidised beds. *Chemical Engineering Science*, 55:5291–5300, 2000.

[83] M. Stein, J. P. K. Seville, and D. J. Parker. Attrition of porous glass particles in a fluidised bed. *Powder Technology*, 100:242–250, 1998.

[84] C. Thornton. (ed.) Foreword. Numerical simulations of discrete particle systems. *Powder Technology* Special Issue, 109:2, 2000.

[85] H. Uhlemann. Kontinuerliche wirbelschicht-sprühgranulation. *Chem.-Ing.-Tech.*, 62(19):822–834, 1990.

[86] M. Vanni. Approximate population balance equations for aggregation-breakage processes. *Journal of Colloid and Interface Science*, 221:143–160, 2000.

[87] B. Waldie. Growth mechanism and the dependance of granule size on drop size in fluidized-bed granulation. *Chemical Engineering Science*, 46(11):2781–2785, 1991.

[88] B. Waldie, D. Wilkinson, and L. Zachra. Kinetics and mechanisms of growth in batch and continous fluidized bed granulation. *Chemical Engineering Science*, 42(4):653–665, 1987.

[89] J. Werther and J. Reppenhagen. Catalyst attrition in fluidized-bed systems. *AIChe Journal*, 45(9):2001–2010, 1999.

[90] P. Wnukowski. *On the coating of particles in fluid-bed granulators.* Dissertation, Royal Institute of Technology, Stockholm, 1989.